



**HAL**  
open science

## T-stubs with two and four bolts under monotonic and cyclic loading

Hichem Rakib Sebbagh, Djamel El Ddine Kerdal, Anis Abidelah, Abdelhamid Bouchaïr

► **To cite this version:**

Hichem Rakib Sebbagh, Djamel El Ddine Kerdal, Anis Abidelah, Abdelhamid Bouchaïr. T-stubs with two and four bolts under monotonic and cyclic loading. *Journal of Constructional Steel Research*, 2021, 178, pp.106486 -. 10.1016/j.jcsr.2020.106486 . hal-03492757

**HAL Id: hal-03492757**

**<https://hal.science/hal-03492757>**

Submitted on 2 Jan 2023

**HAL** is a multi-disciplinary open access archive for the deposit and dissemination of scientific research documents, whether they are published or not. The documents may come from teaching and research institutions in France or abroad, or from public or private research centers.

L'archive ouverte pluridisciplinaire **HAL**, est destinée au dépôt et à la diffusion de documents scientifiques de niveau recherche, publiés ou non, émanant des établissements d'enseignement et de recherche français ou étrangers, des laboratoires publics ou privés.



Distributed under a Creative Commons Attribution - NonCommercial 4.0 International License

# 1 T-stubs with two and four bolts under monotonic and cyclic loading

2 Hichem Rakib Sebbagh <sup>a,b,\*</sup>, Djamel El Ddine Kerdal <sup>a</sup>, Anis Abidelah <sup>c</sup>, Abdelhamid Bouchaïr <sup>b</sup>

3 <sup>a</sup> LM2SC, Civil Engineering Department, U.S.T.O.M.B., B.P. 1505 El M'Naouer, Oran, Algeria

4 <sup>b</sup> Université Clermont Auvergne, CNRS, SIGMA Clermont, Institut Pascal, F-63000 Clermont-Ferrand, France

5 <sup>c</sup> LMST, Civil Engineering Department, U.S.T.O.M.B., B.P. 1505 El M'Naouer, Oran, Algeria

6 <sup>(\*)</sup> corresponding author: tel: +33 (0) 6 19 22 99 23, E-mail address: hichemrakib.sebbagh@univ-usto.dz

7

## 8 Abstract

9 The mechanical behavior of T-stubs bolted connection with two and four bolts per row under  
10 monotonic and cyclic loading is analyzed in this paper using a 3D finite element model. The aim of  
11 the model that takes into account material and geometrical nonlinearities is to obtain the evolution of  
12 prying forces and bolts forces in the T-stubs with four bolts per row throughout the cycles of loading.  
13 The numerical model is also used to compare the behavior of T-stubs with four bolts per row to those  
14 with two bolts per row. The results are prepared to be used as a basis for proposing analytical  
15 mechanical models for bolted endplate connections with four bolts per row using the component  
16 method of Eurocode 3.

## 17 Key words

18 Connection, T-stubs, Four bolts, Cyclic loading, Energy dissipation.

## 19 1. Introduction

20 Steel structures, characterized by high ductility and an excellent mechanical strength to weight ratio,  
21 are well known to withstand seismic actions successfully. However, during the Northridge (USA,  
22 1994) and Hyokogen-Nanbu (Japan, 1995) earthquakes, failures of welded connections were observed  
23 [1-4]. This has led researchers to improve the resistance of existing connections or develop new types  
24 of joints that would withstand seismic forces adequately [5].

25 End-plate connections with two bolts per row have been largely used in steel structures subjected to  
26 high seismic activity [6,7] because of their higher rotational capacity when compared to that of welded  
27 connections. Furthermore, they can be more easily repaired in the case of minor damage preventing  
28 the building from collapsing and enabling thus a quick return to service [8].

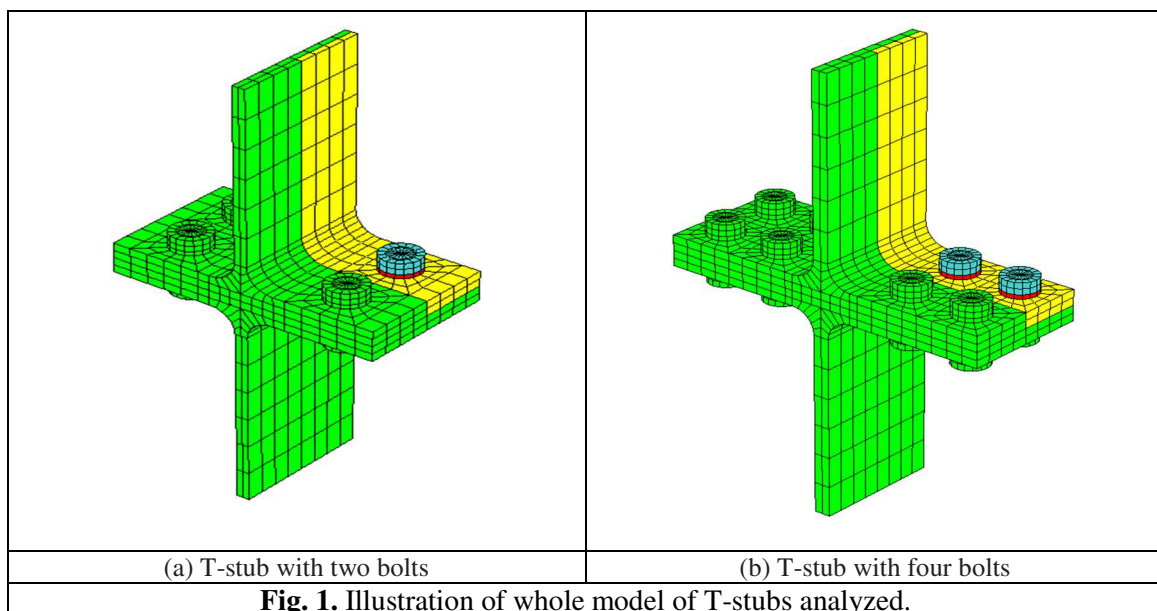
29 Several research works based on experimental and numerical approaches [9-15] have been carried out  
30 in order to identify the behavior of this type of joints under monotonic loading. As a result, an  
31 analytical model based on the Eurocode 3 (EC3) component method [16] has been proposed to  
32 characterize the moment-rotation behavior of end-plate joints with two bolts per row under monotonic  
33 loading. Nevertheless, no standard approach is available to characterize the behavior of these types of  
34 joints under cyclic loading mainly their energy dissipation capacities [17]. This is why several studies  
35 [18-21] have been carried out in order to study the behavior of end-plates connections with two bolts

36 per row under cyclic loads. Nemati et al. [19] conducted an experimental campaign on two groups of  
37 T-stubs with two bolts per row, one was subjected to monotonic loading and the second to cyclic  
38 loading. The authors reported an uplift of the end part of plate of the T-stub subjected to cyclic loads  
39 that modified the contact conditions under the T-stubs flanges. Thus, influencing their mechanical  
40 behavior. Piluso and Rizzano [3] conducted an experimental program on 28 T-stubs with two bolts per  
41 row to obtain their load-displacement response under cyclic loads with constant and variable  
42 amplitudes. The aim was to extend the EC3 component method [16] in order to propose a semi-  
43 analytical model predicting the cyclic behavior of T-stubs with two bolts per row. The authors  
44 concluded that the main parameters describing the degradation of stiffness and strength properties  
45 were the energy cumulated and the displacement amplitude. Iannone et al. [22] and Simões da Silva et  
46 al. [23] proposed an analytical model to describe the behavior of the connections under cyclic loading  
47 based on the EC3 component method [16]. The authors concluded that the global energy dissipation of  
48 the joint can be obtained by adding the dissipated energies of the different components of the cyclic  
49 model. Elsabbagh et al. [24] analyzed numerically the behavior of different configurations of column-  
50 beam connections with stiffened and unstiffened end-plates under monotonic and cyclic loads. The  
51 authors confirmed the conclusions made by Ghobarah et al. [25] considering that the use of end-plate  
52 stiffeners, under cyclic loading, can improve the moment of resistance of the joint. Abidelah et al. [26]  
53 studied the reinforcement of bolted joints by stiffeners on the extended parts of end-plates and  
54 concluded that the presence of stiffeners enhanced the strength of the connections but reduced the  
55 ductility. However, the use of stiffeners with a concrete slab or steel deck is difficult [27]. Although  
56 this type of reinforcement is commonly used in seismic zones [28], recent research suggested that the  
57 using stiffeners should be avoided because of the stress concentrations at the joint zone [29]. In  
58 addition, the current Eurocode 8 (EC8) regulation [30] recommends that the joints should develop a  
59 dissipative behavior in areas with seismic activity.

60 In recent years, several studies have been conducted in order to analyze the behavior of T-stubs with  
61 four bolts per row under monotonic loading [31-34]. The authors concluded that there was an increase  
62 in the strength and the stiffness of the connections when compared to those of two-row bolt joints  
63 while still remaining easy to assemble on sites. In addition the outer bolts provide an additional safety  
64 in the eventuality of failure arising in the inner bolts. However, EC3 [16] in its current version does  
65 not provide recommendations for the design of joints with four bolts per row. To this effect,  
66 Demonceau et al. [32] have proposed an analytical model to evaluate the strength and stiffness of the  
67 T-stubs with four bolts per row based the component method [16]. Latour et al. [33] have also  
68 experimentally and numerically analyzed the behavior of three T-stub configurations with four bolts  
69 per row in order to obtain the three typical failure modes of T-stubs. The authors reached to the  
70 conclusion that the geometric configurations of T-stubs, that influence the failure mode, had an effect  
71 on the participation of the outer bolts to the overall resistance of the connections. Haouas et al. [34]

72 numerically and analytically analyzed the behavior of T-stubs with four bolts per row under  
73 monotonic loading. The authors concluded that for some configurations, the outer bolts are not loaded  
74 and that the prying force was applied between the inner and outer bolts, thereby reducing considerably  
75 the contribution of the outer bolts to the resistance of the joint.

76 The aim of this paper is to analyze numerically the behavior of T-stub with two (Fig. 1a) and four  
77 bolts (Fig. 1b) per row under monotonic and cyclic loading. Both the global load-displacement curves  
78 and the evolution of the bolt forces by considering the prying forces were analyzed. All the T-stubs  
79 configurations were modeled using the finite elements software CAST3M [35]. The mesh densities  
80 were selected on the basis of convergence study and the evaluation of symmetry conditions effect  
81 (Figs. 2 and 3). **The load-displacement curves obtained by the numerical model represent well  
82 those of experimental tests under monotonic and cyclic loading available in the literature [3] [36,  
83 37]. The models, validated on the T-stubs with two bolts per row under monotonic loads (Fig. 2),  
84 were then used as basis for the T-stubs with four bolts per row (Fig. 3).** The results of the T-stubs  
85 with two bolts per row, under monotonic and cyclic loads, were also used as reference to evaluate the  
86 contribution of the outer bolts in the T-stub with four bolts. The behavior of T-stubs with four bolts  
87 per row under cyclic loading was analyzed and compared to that with two bolts per row on the basis of  
88 load-displacement curves and key parameters given by the European convention for constructional  
89 steelwork (ECCS) [38]. The analysis also included the evolution of prying effects and bolt forces with  
90 special focus on the outer bolts.



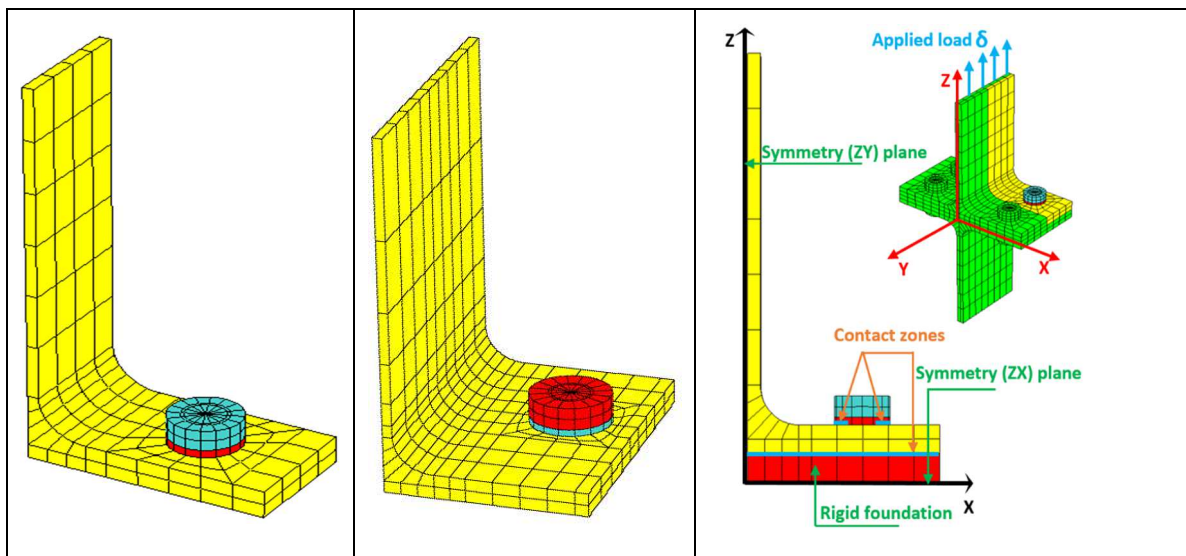
91

## 92 2. Monotonic behavior of T-stubs with two and four bolts per row

### 93 2.1. Numerical modeling

94 2.1.1. Description of the numerical model

95 A three-dimensional finite element model using Cast3m [35] was developed to predict the monotonic  
96 and cyclic behavior of T-stubs with two and four bolts per row. Solid elements with twenty nodes  
97 (CU20) were used to model one eighth of the T-stubs by considering three planes of symmetry as  
98 shown in Figs. 2 and 3. This solid element that has been selected after testing different types of  
99 elements and mesh densities has been found to give a good compromise between the size of the  
100 elements and the stability of the numerical solution adopted [39,40]. The model considers two sources  
101 of non-linearity: the plastic behaviour of materials and the contact evolution between the different  
102 parts of the T-stub. This model has been adapted to take into account the non-uniform distribution of  
103 nodal forces between the corner nodes and the median nodes of the elements by introducing a further  
104 condition on nodal displacements between the central node and the corner nodes over the full  
105 boundary of all elements on the contact surfaces. However, although the ZX and ZY are geometric  
106 symmetry planes, the XY plane does not satisfy the symmetry condition since the elongation of the  
107 bolt is unsymmetrical in the Z direction. To this effect, some authors [41] proposed to replace the real  
108 bolt by “an equivalent bolt” whose geometrical stiffness was identical to that of the actual bolt and  
109 complied with the requirements for symmetry in the XY plane and with an elongation equal to half  
110 that of the actual bolt [42]. This model was simplified by using a cylinder of constant nominal  
111 diameter with a washer of the same diameter as the head of the bolt. Boundary conditions were taken  
112 into consideration by defining symmetry on the nodes of ZX and ZY planes and by using contact in  
113 the XY plane between bolt head and flange surface as well as between flange and symmetrical part  
114 (foundation) (Figs. 2c and 3c). In order to reduce the number of contact planes, bolt head is considered  
115 completely connected to the washer. Contact calibration for the model was carried out based on a  
116 Hertz contact example which analytical solution has been well known. Lagrange multipliers to model  
117 unilateral frictionless contact were used in each contact area. Load has been applied at the top of the  
118 T-stubs in the Z-direction using displacement control (Figs. 2c and 3c).



(a) Specimen $T_{b1-M12}$	(b) Specimen $T_{g1-M16}$	(c) Contact zones
---------------------------	---------------------------	-------------------

**Fig. 2.** Meshing of the two-bolt T-stubs and the contact zones.

119

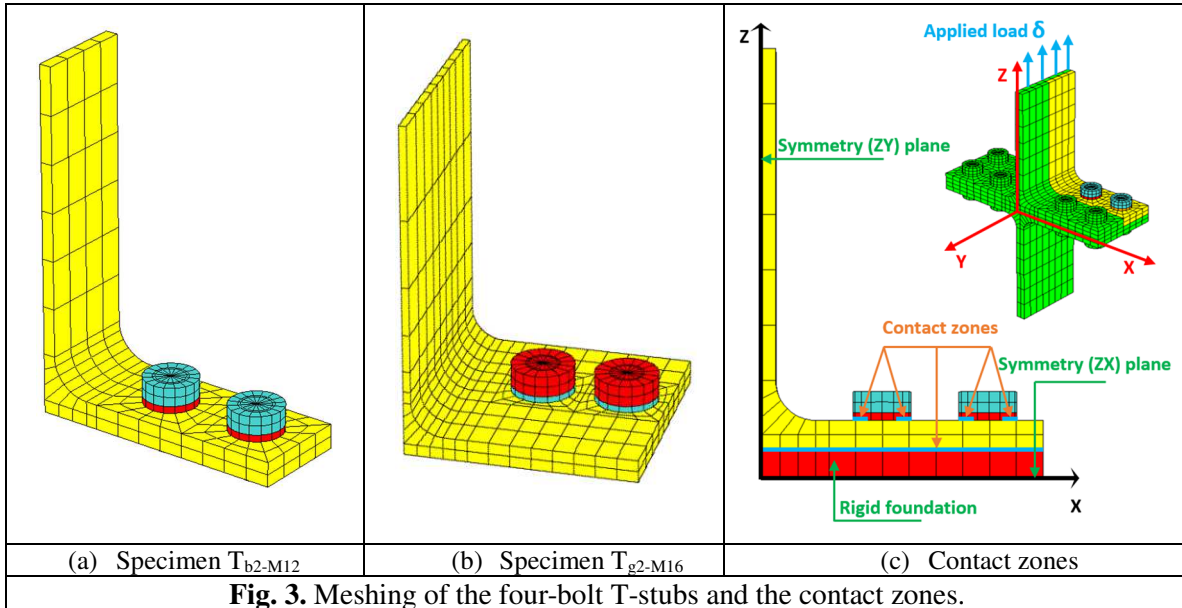
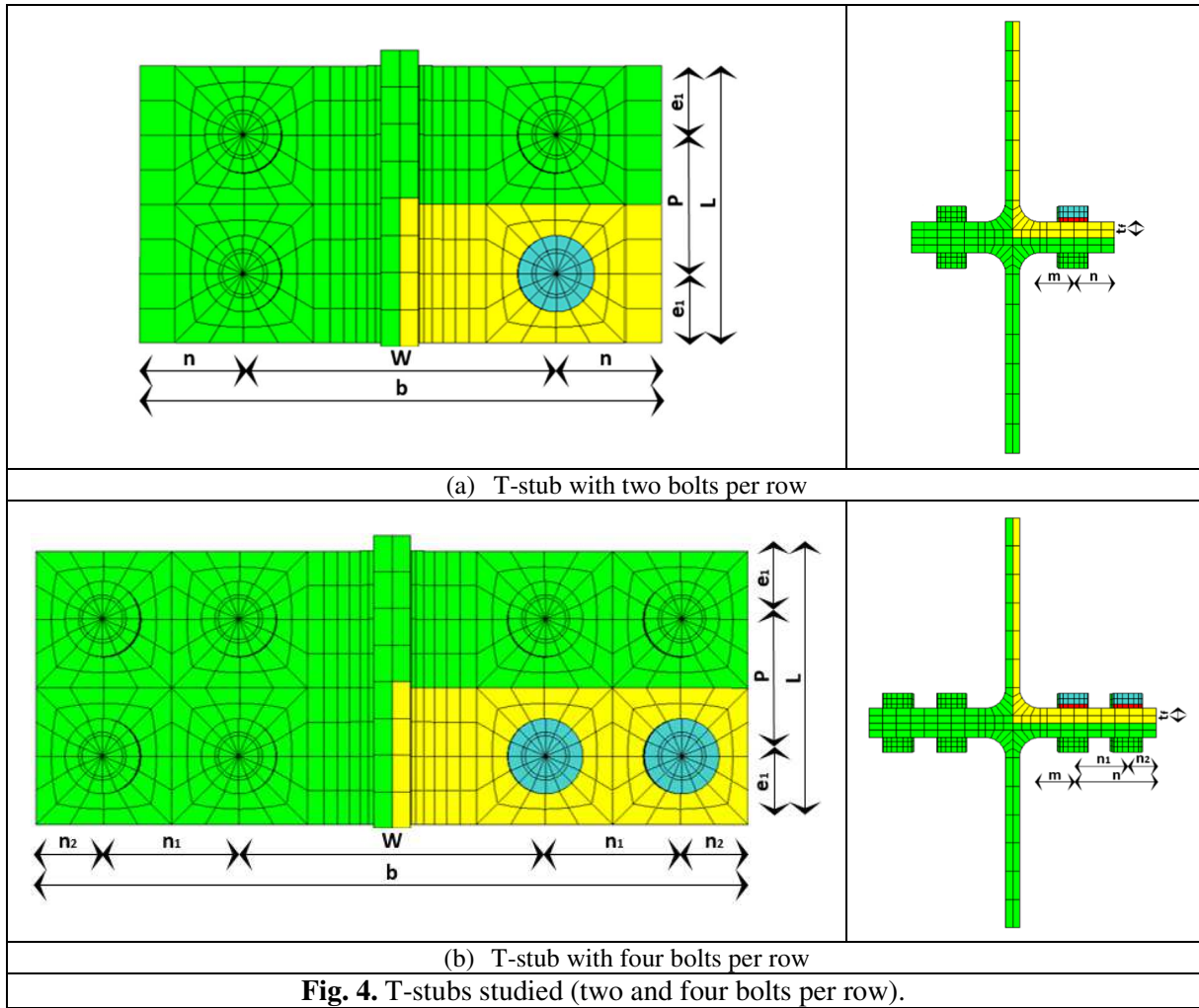


**Fig. 3.** Meshing of the four-bolt T-stubs and the contact zones.

120

121 In order to validate the numerical models, two T-stubs with different mechanical and geometrical  
122 characteristics were modeled. These are symmetrical T-stubs with two bolts per row, named  $T_{b1\_M12}$   
123 (Fig. 2a) and  $T_{g1\_M16}$  (Fig. 2b), whose experimental results are available from the literature [36,37].  
124 The T-stubs taken from hot-rolled IPE300 profiles are symmetrical with two rows of two bolts (Fig.  
125 4a). The geometrical characteristics of the T-stubs are given in Table 1. M12 Bolts of grade 8.8 and  
126 M16 of grade 10.9 are used for T-stub  $T_{b1\_M12}$  and for T-stub  $T_{g1\_M16}$  respectively. The dimensions and  
127 the mechanical characteristics of the T-stubs are given in Table 1. After validation of the numerical  
128 models, the models of T-stubs with four bolts per row, named  $T_{b2\_M12}$  (Fig. 3a) and  $T_{g2\_M16}$  (Fig. 3b),  
129 are made from the T-stubs with two bolts by referring to the spacing conditions given by EC3 [16]  
130 (Fig. 4b). The dimensions considered are given in Table 1. The mechanical characteristics considered  
131 for the T-stubs  $T_{b2\_M12}$  and  $T_{g2\_M16}$  are those used for the T-stubs  $T_{b1\_M12}$  and  $T_{g1\_M16}$ . The stress–strain  
132 curves of steel used in the numerical models are built from the real values of the yield and ultimate  
133 limits of the plates (Fig. 5a) and bolts (Fig. 5b). **In addition, the 4-bolt numerical models have been**  
134 **validated in accordance with the T-stubs that were experimentally tested by Latour et al [33].** It  
135 has to be noted that in order to allow a direct comparison between the numerical and experimental  
136 results, the load applied to the T-stubs has been multiplied by 2 and therefore the force in the bolts is  
137 multiplied by 4 for all numerical results.

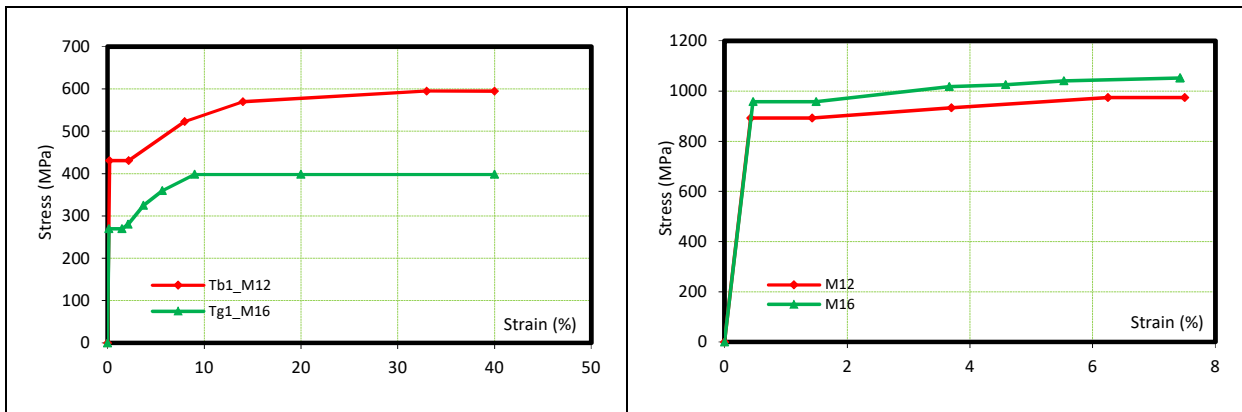


138

**Table 1**  
Geometrical and mechanical characteristics of T-stubs used in the finite element model.

T-stubs	Plate $f_{y,t}/f_{u,t}$ (MPa)	Bolts $f_{y,b}/f_{u,b}$ (MPa)	Dimensions (mm)									
			P	$t_f$	W	L	b	$e_1$	m	n	$n_1$	$n_2$
T <sub>b1_M12</sub>	431/595	2*2 M12-8.8 $f_{y,t}/f_{u,t} = 893/974$	40	10.7	90	80	150	20	29.4	30	/	/
T <sub>g1_M16</sub>	270/398	2*2 M16-10.9 $f_{y,t}/f_{u,t} = 957/1052$	90	10.7	100	210	150	60	34.4	25	/	/
T <sub>b2_M12</sub>	431/595	4*2 M12-8.8 $f_{y,t}/f_{u,t} = 893/974$	40	10.7	90	80	210	20	29.4	60	40	20
T <sub>g2_M16</sub>	270/398	4*2 M16-10.9 $f_{y,t}/f_{u,t} = 957/1052$	90	10.7	100	210	210	60	34.4	60	40	20

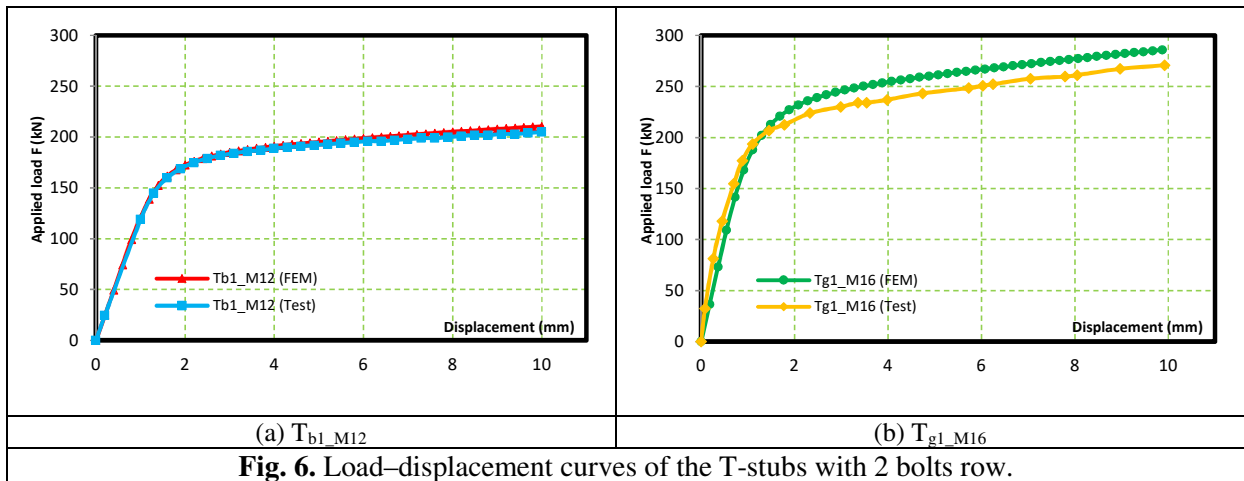
139



(a) Plates	(b) Bolts
<b>Fig. 5. Stress-strain curves used in the finite element model.</b>	

140

141 The numerical and experimental load-displacement curves ( $F-\delta$ ) of T-stubs  $T_{b1\_M12}$  and  $T_{g1\_M16}$  under  
 142 monotonic loading are compared in Fig. 6. Comparative results show a high correlation between the  
 143 experimental tests and the numerical models regarding initial stiffness and strength. Superimposing  
 144 the curves shows that the numerical models developed provide a good representation of the real  
 145 behavior of T-stubs.



146

147 2.2. Analysis of the results

148 2.2.1. Monotonic load response

149 The monotonic load-displacement curves ( $F-\delta$ ) of the T-stubs with two bolts ( $T_{b1\_M12}$  and  $T_{g1\_M16}$ ) and  
 150 the T-stubs with four bolts ( $T_{b2\_M12}$  and  $T_{g2\_M16}$ ) are compared in Fig. 7. Superimposing the curves of  
 151 the  $T_{b1\_M12}$  and  $T_{b2\_M12}$  T-stubs and the  $T_{g1\_M16}$  and  $T_{g2\_M16}$  T-stubs shows that T-stubs with four bolts are  
 152 characterized by a higher rigidity compared to T-stubs with two bolts. Furthermore, by adding outer  
 153 bolts, the same imposed displacement requires 15% more applied load than for T-stubs with two bolts  
 154 per row.

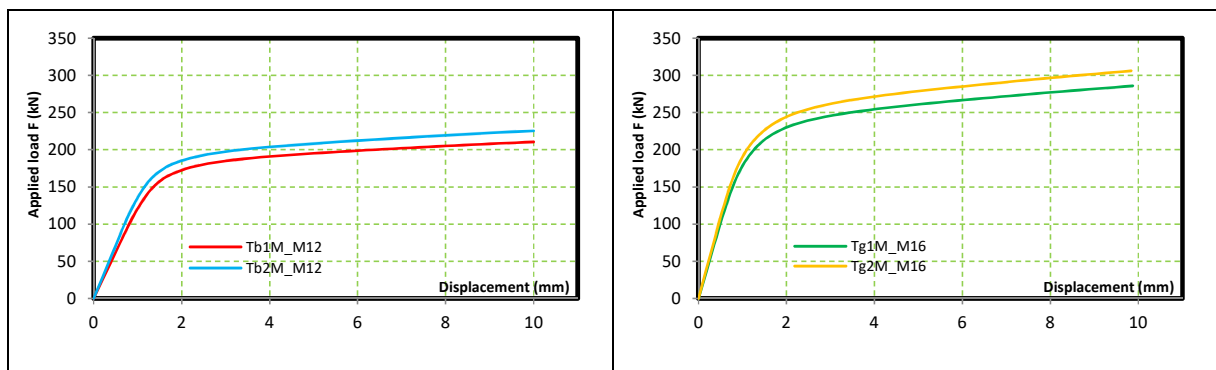


**Fig. 7.** Load–displacement curves of the T-stubs comparing 2 and 4 bolts row.

155

156 2.2.2. Prying action and forces in the bolts

157 The curves of Fig. 8 that give the variations of the prying forces ( $F_Q$ ) as a function of applied force ( $F$ )  
158 for T-stubs with 2 bolts ( $T_{b1\_M12}$  and  $T_{g1\_M16}$ ) and T-stubs with 4 bolts ( $T_{b2\_M12}$  and  $T_{g2\_M16}$ ) show that  
159 there is a linear increase of the prying forces until the flange starts yielding. For values of applied load  
160 equal to 180, 230, 190 and 250kN respectively for the sections  $T_{b1\_M12}$ ,  $T_{g1\_M16}$ ,  $T_{b2\_M12}$  and  $T_{g2\_M16}$ , all  
161 T-stubs reached a complete yielding of the flange. At the stage, a rapid increase of the prying forces is  
162 observed.

163 Variations in bolt forces as a function of the applied force ( $F$ ) given in Fig. 9, for T-stubs with two  
164 bolts ( $T_{b1\_M12}$  and  $T_{g1\_M16}$ ) and four bolts ( $T_{b2\_M12}$  and  $T_{g2\_M16}$ ), show that the bolts in the T-stubs with  
165 two bolts behave in a similar way as the inner bolts of T-stubs with four bolts. The outer bolts are not  
166 subjected to any load during the elastic phase of loading. However, after complete flange yielding  
167 (failure mode 1), the outer bolts of T-stubs start to take up loads that remain low compared to the load  
168 taken up by the inner bolts (about 1% for  $T_{b2M\_M12}$  and 10% for  $T_{g2M\_M16}$ ). The difference between the  
169 behaviors of the outer bolts of the T-stub  $T_{b2M\_M12}$  and  $T_{g2M\_M16}$  is due to the position of bolts of the T-  
170 stub  $T_{g2M\_M16}$  that is not centered, causing thus a bi-axial bending of the plate. As a general  
171 observation, in case of a weak plate and strong bolt (failure mode 1) the outer bolts being in the area of  
172 the plate that remains undeformed, do not contribute to the T-stub resistance [33]. Nevertheless, in the  
173 case there is a bi-axial bending of the T-stub plate, the outer bolts contribute to the T-stub resistance.

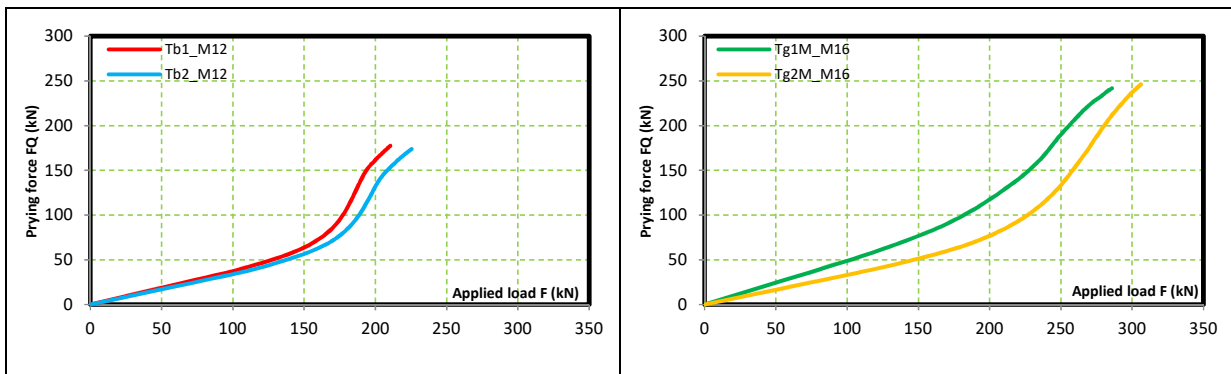


**Fig. 8.** Prying force vs. the applied load for T-stubs with 2 and 4 bolts row.

174

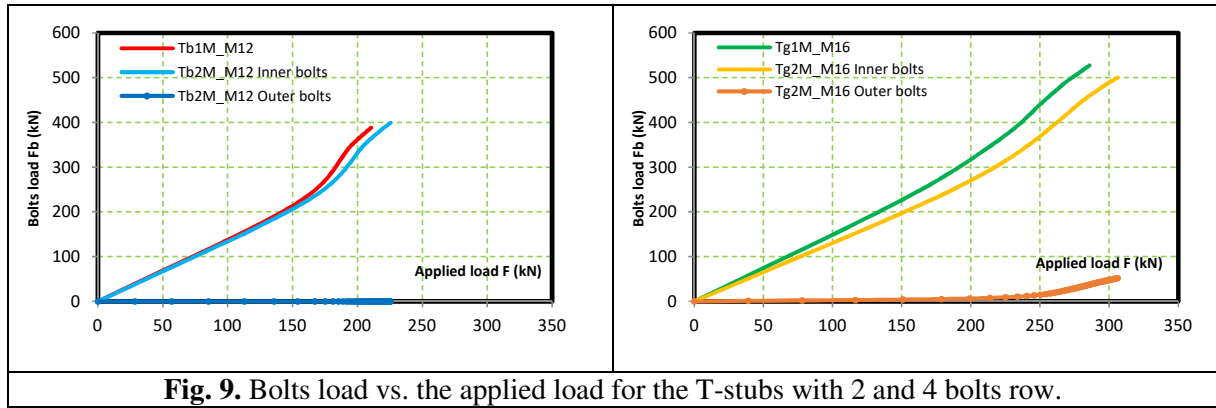


**Fig. 9.** Bolts load vs. the applied load for the T-stubs with 2 and 4 bolts row.

175

176 **3. Cyclic behavior of T-stub with two and four bolts per row**

177 3.1. Cyclic Loading history

178 Cyclic loading that is based on the ECCS recommendations [38] is governed by the value of the  
 179 conventional elastic displacement  $\delta_y$  that corresponds to the elastic resistance ( $F_y$ ) that is given by the  
 180 intersection between the two tangent lines of the load–displacement curve of the T stubs at the initial  
 181 and the final stages of the monotonic load (Fig. 10). The loading protocol starts with four cycles of  
 182 loading at different amplitudes with an increment equal to  $(\delta_y/4)$  until the value of the displacement  $\delta_y$   
 183 is reached. Whereby, the ECCS [38] recommends to repeat the same displacement three times for each  
 184 cycle with values of increments given by the formula  $(2+2n) \delta_y$  with  $(n = 0, 1 \text{ and } 2)$  (Fig. 11). Due to  
 185 their design and symmetry, T-stubs are subjected to repeated cyclic loading with an imposed positive  
 186 displacement.

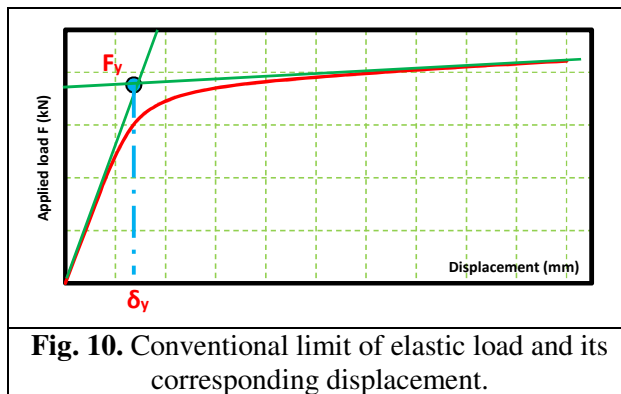


**Fig. 10.** Conventional limit of elastic load and its corresponding displacement.

187

188

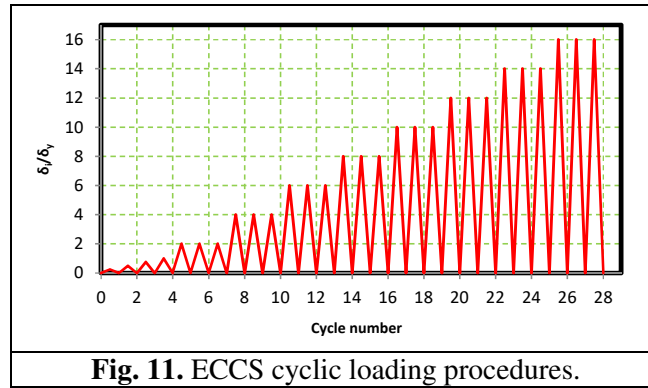


Fig. 11. ECCS cyclic loading procedures.

189 On the basis of the recommendations of the ECCS [38], the values of the conventional elastic  
190 displacement  $\delta_y$  obtained from the numerical curves  $F-\delta$  under monotonic loads (Fig. 12) are equal to  
191 1.3mm for the T-stubs  $T_{b1\_M12}$ ,  $T_{b2\_M12}$  and  $T_{g2\_M16}$  and 1.2mm for the T-stub  $T_{g1\_M16}$  that correspond  
192 respectively to values of applied load equal to 180kN, 190kN, 250kN and 230kN respectively.

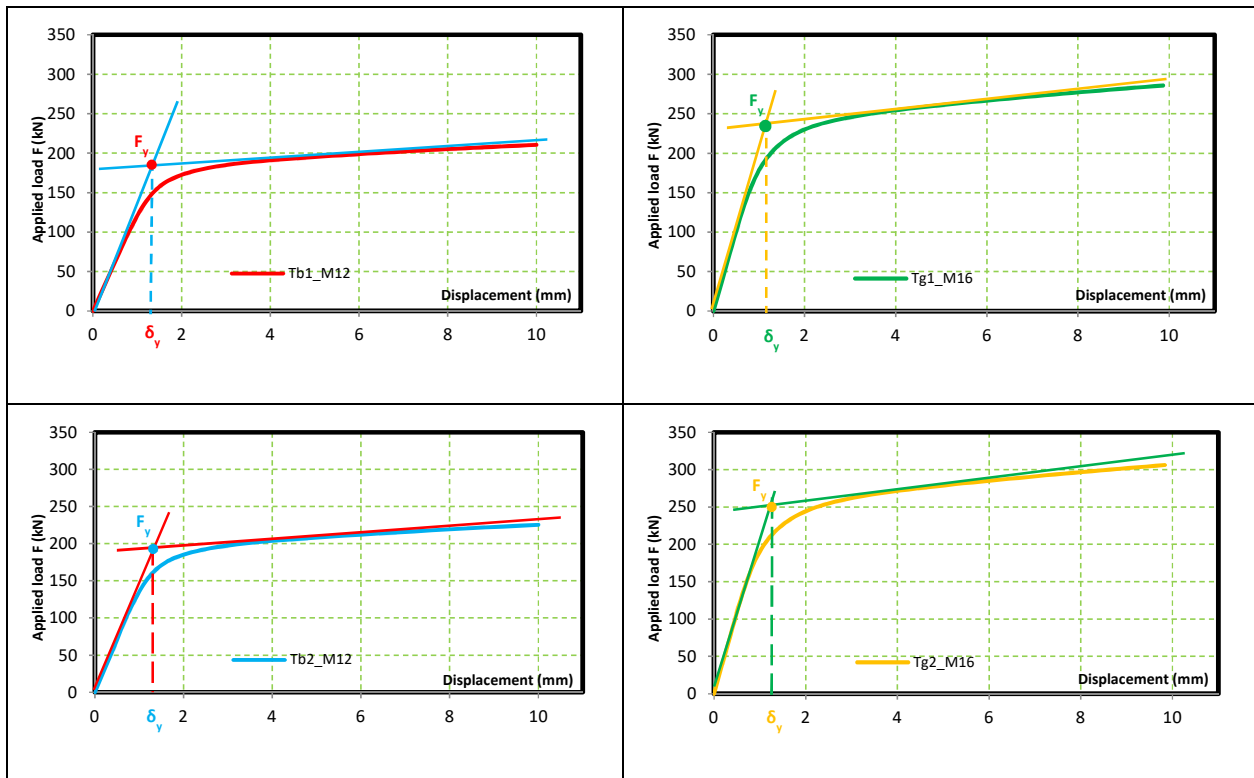


Fig. 12. Conventional limit of elastic range and its corresponding displacement for the T-stubs with 2 and 4 bolts row.

193

### 194 3.2. Cyclic model validation

195 The validation of the numerical model under cyclic loading by considering different collapse  
196 mechanisms is performed to characterize the real T-stubs hysterical behavior. Thus, two T-stubs  
197 with different mechanical and geometrical characteristics were modeled. These are symmetrical  
198 T-stubs with two M20 bolts per row, of grade 8.8, named A3 (Fig. 13a) and B7 (Fig. 13b), whose

199 experimental results are available from the literature [3]. The T-stubs A3 and B7 that were cut  
 200 respectively from hot-rolled HEA180 and HEB180 sections have different collapse mechanisms  
 201 (A3: Mode 1 and B7: Mode 2). The geometrical and mechanical characteristics of the T-stubs  
 202 are given in Table 2. The cyclic loading has been carried out by considering respectively 10 and  
 203 13 cycles of constant amplitude of 20mm for A3 and B7.  
 204

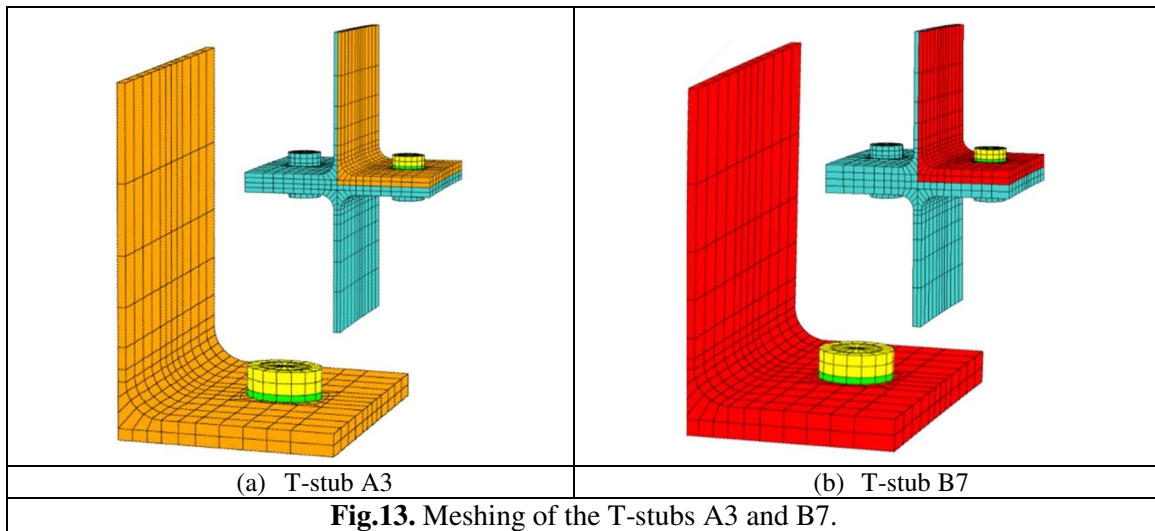


Fig.13. Meshing of the T-stubs A3 and B7.

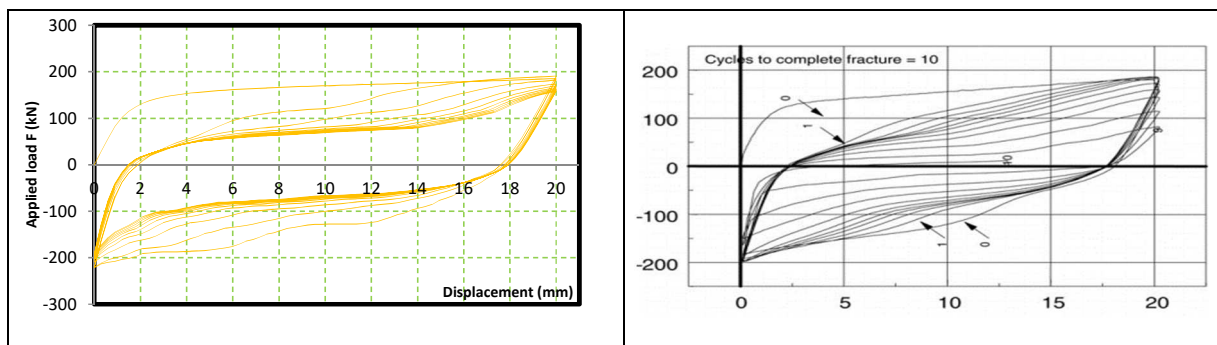
205

**Table 2**  
 Geometrical and mechanical characteristics of T-stubs used in the modeling

T- stub	Plate $f_{y,t}/f_{u,t}$ (MPa)	Bolts $f_{y,b}/f_{u,b}$ (MPa)	$t_f$	$t_w$	Dimensions (mm)					
					W	L	b	$e_1$	m	n
A3	334.67/530.62	2*1 M20-8.8 $f_{y,t}/f_{u,r} = 640/800$	9.79	9.79	105.65	158.75	181.50	79.38	37.51	37.93
B7	280.10/464.56	2*1 M20-8.8 $f_{y,t}/f_{u,r} = 640/800$	14.01	14.01	105.67	158.75	179.75	79.38	36.81	37.04

206

207 The numerically obtained hysteretic load-displacement curves ( $F-\delta$ ) of the T-stubs A3 and B7  
 208 were compared to the experimental ones in Fig. 14. The comparison shows that the numerical  
 209 model describes satisfactorily the real hysterical behavior of the T-stubs during all loading  
 210 cycles but could not predict their deterioration of strength and stiffness prior to the complete  
 211 fracture because the model was designed with elastic-plastic analysis and contact without  
 212 damage evolution.



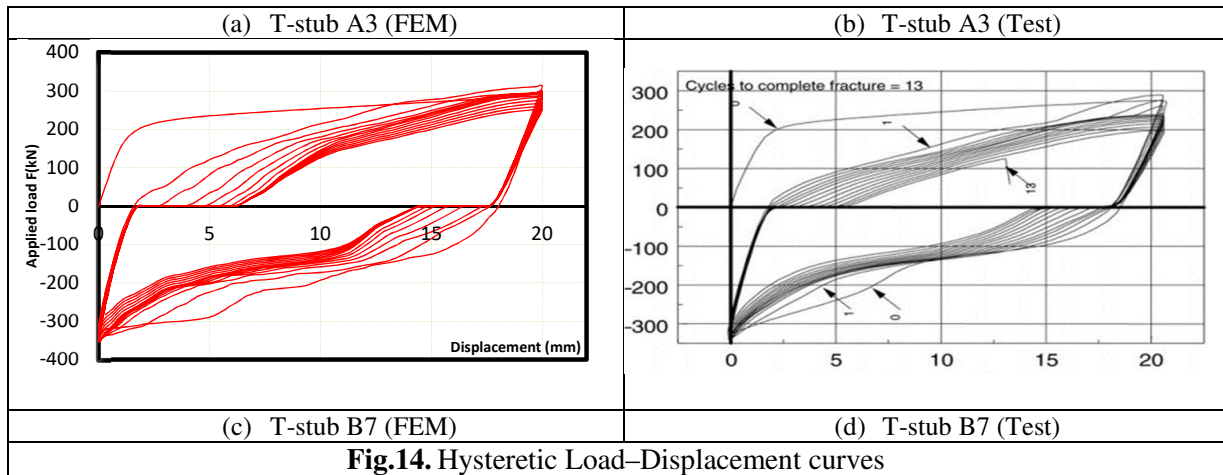


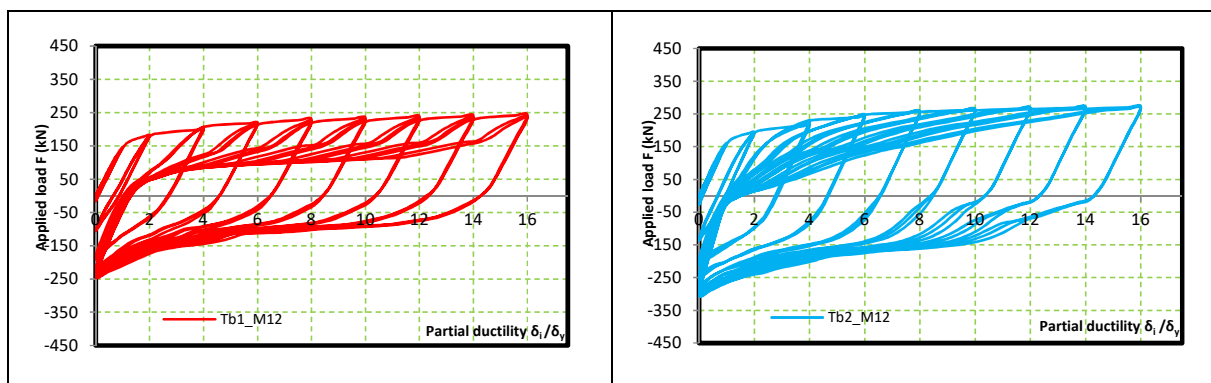
**Fig.14.** Hysteretic Load–Displacement curves

213

214 3.3. Analysis of the results

215 3.3.1. Hysteretic load–displacement response

216 The hysteretic load-displacement curves ( $F-\delta$ ) under cyclic loading of the T-stubs with two ( $T_{b1C\_M12}$ ,  
 217  $T_{g1C\_M16}$ ) and four bolts per row ( $T_{b2C\_M12}$  and  $T_{g2C\_M16}$ ) obtained numerically are plotted in Fig. 15  
 218 versus the partial ductility as defined by the relation  $(\delta_i/\delta_y)$  [38]. Although the hysteretic  $F-\delta$  curves of  
 219 the T-stubs with two bolts and four bolts per row are similar in shape, the comparison between the  $F-\delta$   
 220 hysteresis curves of all T-stubs shows that the hysteresis curves of the T-stubs with four bolts are  
 221 being wider and more stable than those with two bolts. In addition, the  $F-\delta$  hysteresis curves of the T-  
 222 stubs with two bolts per row are characterized by a significant decrease in stiffness at the beginning of  
 223 each loading cycle for the imposed displacement values  $\delta_i > \delta_y$ . **As a result, 4-bolt T-stubs  $T_{b2c\_M12}$**   
 224 **and  $T_{g2c\_M16}$  have respectively about 10 and 15% greater strength than the 2-bolt T-stubs**  
 225 **subjected to cyclic loads as well as preventing a significant variation and decrease in stiffness.**



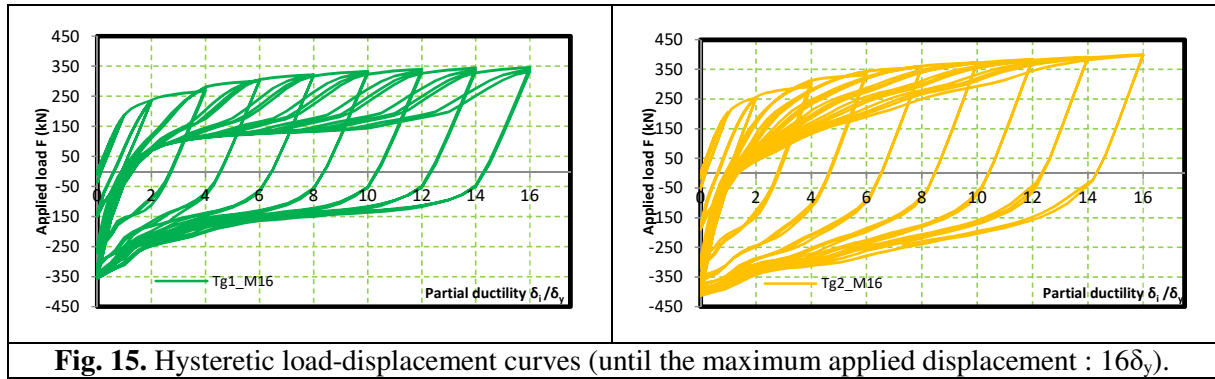


**Fig. 15.** Hysteretic load-displacement curves (until the maximum applied displacement :  $16\delta_y$ ).

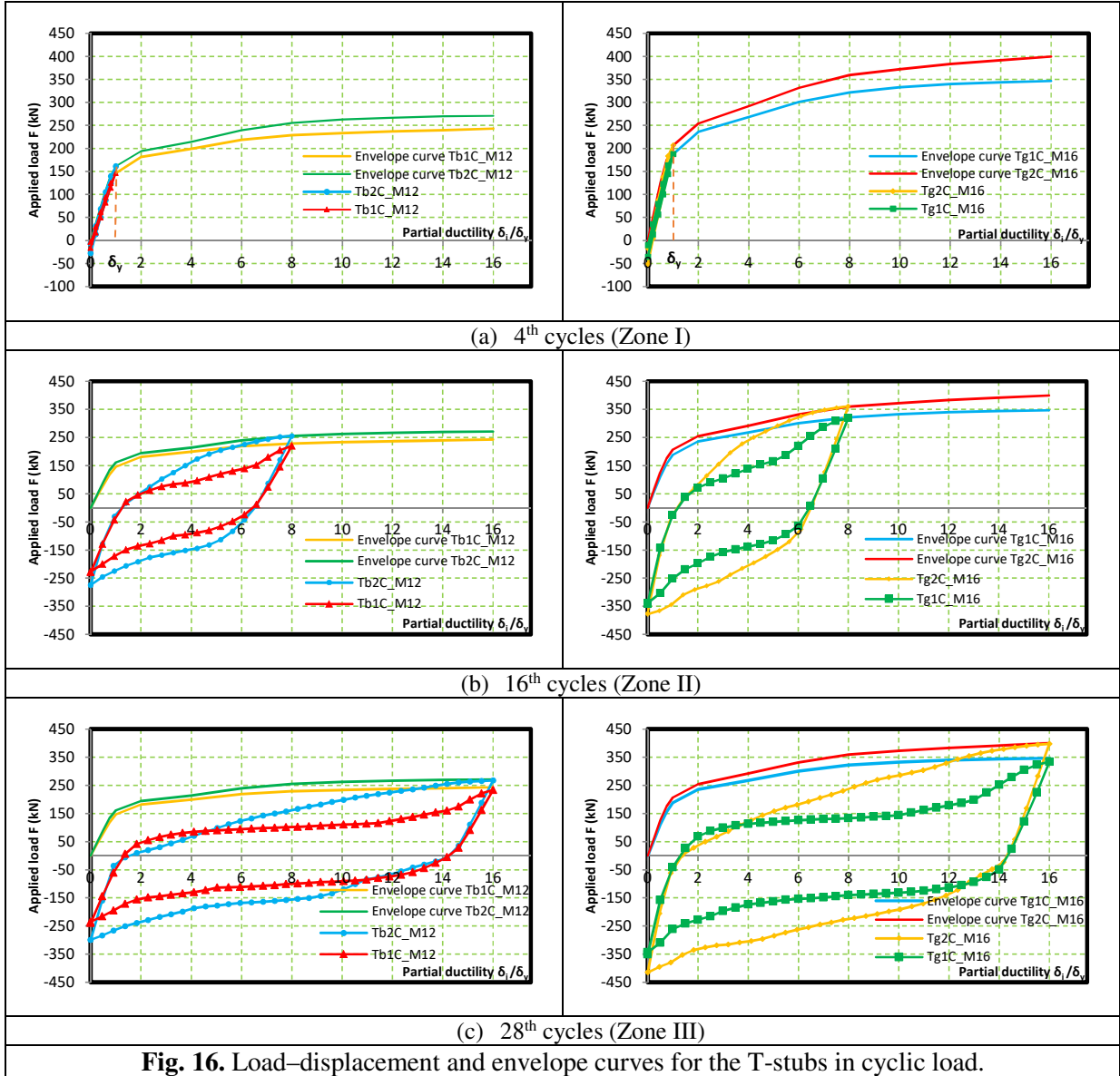
226

227 Three zones can be defined by observing the shapes of the hysteretic  $F$ - $\delta$  curves shown in Fig. 15 of  
 228 the T-stubs with two bolts per row. Zone I is defined for a value of displacement less or equal to  $\delta_y$   
 229 that corresponds to the first four cycles of loading (elastic domain) where no decrease in stiffness is  
 230 observed on the hysteretic  $F$ - $\delta$  curves. The zone II is defined from the 5<sup>th</sup> to the 16<sup>th</sup> loading cycle  
 231 corresponding to a maximum imposed displacement value equal to  $8\delta_y$  where the stiffness of  
 232 hysteretic  $F$ - $\delta$  curves of the T-stubs with two bolts per row starts to decrease. Finally, zone III is  
 233 defined beyond the 16<sup>th</sup> loading cycle until the 28<sup>th</sup> loading cycle corresponding to a maximum  
 234 imposed displacement value equal to  $16\delta_y$ . In this last zone, the hysteretic  $F$ - $\delta$  curves of the T-stubs  
 235 with two bolts per row are characterized by a clear decrease in stiffness at the beginning of each cycle.

236 The hysteretic loops of the last cycle of each zone of T-stubs with two and four bolts per row and their  
 237 positioning with regard to the corresponding envelope curve are compared in Fig. 16. In zone I, the  
 238 hysteresis loops of all four T-stubs have a stable linear shape (Fig. 16a) because the T-stubs are still  
 239 loaded in the elastic domain. However, in the case of the sections with four bolts per row the initial  
 240 stiffness and applied load are greater by about 15% as compared to those of the T-stubs with two bolts  
 241 per row (Table 3). In zones II and III (Figs. 16b and c), the hysteretic loops of the T-stubs with two  
 242 bolts per row are characterized by a decrease in stiffness at the beginning of the cycle, this decrease  
 243 being more important in zone III (Fig. 16c), due to the more pronounced yielding of the plate.  
 244 However, the hysteretic loops of the T-stubs with four bolts per row show no significant decrease in  
 245 stiffness. The decrease in stiffness observed in the hysteretic loops of the T-stubs with two bolts  
 246 indicates that this configuration is prone to a change in its mechanical behavior due to the fact that the  
 247 contact starts to be lost between the foundation and the plate. Indeed, the plate behaves like a  
 248 cantilever due to the uplift of its end part during the unloading phase. Thus, this decrease in rigidity is  
 249 associated with the temporary cancellation of the prying forces. At the start of the cycle, this decrease  
 250 in stiffness results in an applied load difference of about 70% (Table 3) between the T-stubs with two  
 251 bolts and those with four bolts per row in Zone II. This difference becomes more significant in zone  
 252 III, where it reaches a difference in value equal to about 85% (Table 3). The difference in applied load  
 253 between the T-stubs with two and four bolts expressed by  $\Delta F$  given by Eq. (1) is shown in Table 3.

254 Furthermore, the addition of the outer bolts improves the shape of the hysteresis loops that become  
 255 wider and more stable. This qualitative improvement of the hysteresis loops resulting in a greater  
 256 energy dissipation [18].

$$257 \quad \Delta F = \frac{F(T_{stub\_4bolts}) - F(T_{stub\_2bolts})}{F(T_{stub\_2bolts})} \quad (1)$$



258

**Table 3**  
 Difference in applied load between the T-stubs with 2 and 4 bolts.

Zone	Cycle number	$\delta_y/\delta_y$	$T_{b2c\_M12}$ (kN)	$T_{b1c\_M12}$ (kN)	$\Delta F$ %	$T_{g2c\_M16}$ (kN)	$T_{g1c\_M16}$ (kN)	$\Delta F$ %
I	4	0,5	87	75	16	115	101	14
		1	162	146	11	207	188	10
II	16	4	161	92	75	236	139	70
		8	256	220	16	361	318	14

		8	161	101	60	235	134	75
<b>III</b>	<b>28</b>	12	226	125	81	332	179	85
		16	268	234	15	398	334	19

259

260 In addition to the significant decrease in stiffness and strength in Zone III, the hysteretic loops in the  
261 T-stubs with two bolts per row are characterized by a more pronounced variation in stiffness. For this  
262 purpose, the hysteretic loop of the 28<sup>th</sup> loading cycle of the T-stub  $T_{blc\_M12}$  has been idealized by ten  
263 straight lines each with different slopes according to the different stiffnesses observed. These and the  
264 deformed shapes of the plate and bolts corresponding to the different stiffnesses are shown in Figs. 17  
265 and 18. The first two stiffnesses observed on the hysteretic loop during Step1 and Step2 (Fig. 17),  
266 correspond to the start of a new loading cycle. These first steps are characterized by the progressive  
267 lifting of the plate on fillet radius side under the effect of the applied loading ( $F$ ) and the uplift of its  
268 end part as a result of the unloading of the previous cycle (Figs. 18a and b). As a result of this uplift,  
269 the contact pressures that are at the origin of the prying forces ( $F_Q$ ) are positioned between the bolt  
270 axis and the fillet radius in Step1 (Fig. 18a) and are tending to move towards the bolt axis in the  
271 second step (Step2) (Fig. 18b). This explains the difference in stiffness between the two steps. As a  
272 result of the deformation of the bolts due to their bending during the preceding cycles, only a contact  
273 between the bolt head on the end part of plate and the plate is generated thus resulting in a reduction of  
274 the bolt forces ( $F_b$ ). During step 3 (Fig. 17) the contact between the bolt head and the plate remains  
275 unchanged. However, no contact is generated between the plate and the foundation (Fig. 18c), thus  
276 temporarily canceling the contact pressure under the plate that would have created the prying forces  
277 and explaining the significant decrease in rigidity observed on the hysteretic loop (Fig. 17).  
278 Subsequently, a new increase of rigidity is observed in Step4 (Fig. 17) that is due to the bending of the  
279 plate and its significant lifting on the fillet radius side that restore the full contact between the head of  
280 the bolt and the plate (Fig. 18d). In Step 5 the end part of plate and the foundation (Fig. 18e) are again  
281 in full contact, the prying forces reappear, resulting in a rapid increase in rigidity (Fig. 17) before the  
282 start of the unloading operation. During step 6 when there is elastic unloading, the prying action ( $F_Q$ )  
283 becomes a compressive force under the base plate ( $R_Q$ ) (Fig. 18f). Subsequently, in step 7, due to the  
284 deformations of the plate and the bolt in bending, a progressive loss of contact between the head of the  
285 bolt and the plate is observed on the fillet radius side (Fig. 18g), as a result of the flattening of the  
286 plate under the effect of the unloading, thus reducing the forces in the bolts and leading to a decrease  
287 in the rigidity (Fig. 17). During Step 8 (Fig. 17), a total loss of contact between the bolt head and the  
288 plate is observed (Fig. 18h), causing a temporary cancellation of the bolt forces and a significant  
289 decrease in stiffness. In addition, during steps 7 and 8, the compressive force ( $R_Q$ ) tends to move  
290 toward the bolt axis (Figs. 18g and h). Finally, the last two stiffness increases corresponding to steps 9  
291 and 10 (Fig. 17), are characterized by the uplifting of the end part of the plate, thus generating a  
292 contact between the bolt head on the end part side and the plate. Consequently, in step 9 the forces in

293 the bolts appear again (Fig. 18i), thus explaining the first increase in stiffness. The final step in the  
 294 loop (Step 10) is characterized by the recovery of the full contact between the plate on the fillet radius  
 295 side and the foundation (Fig. 18j) that explains the additional increase in stiffness.

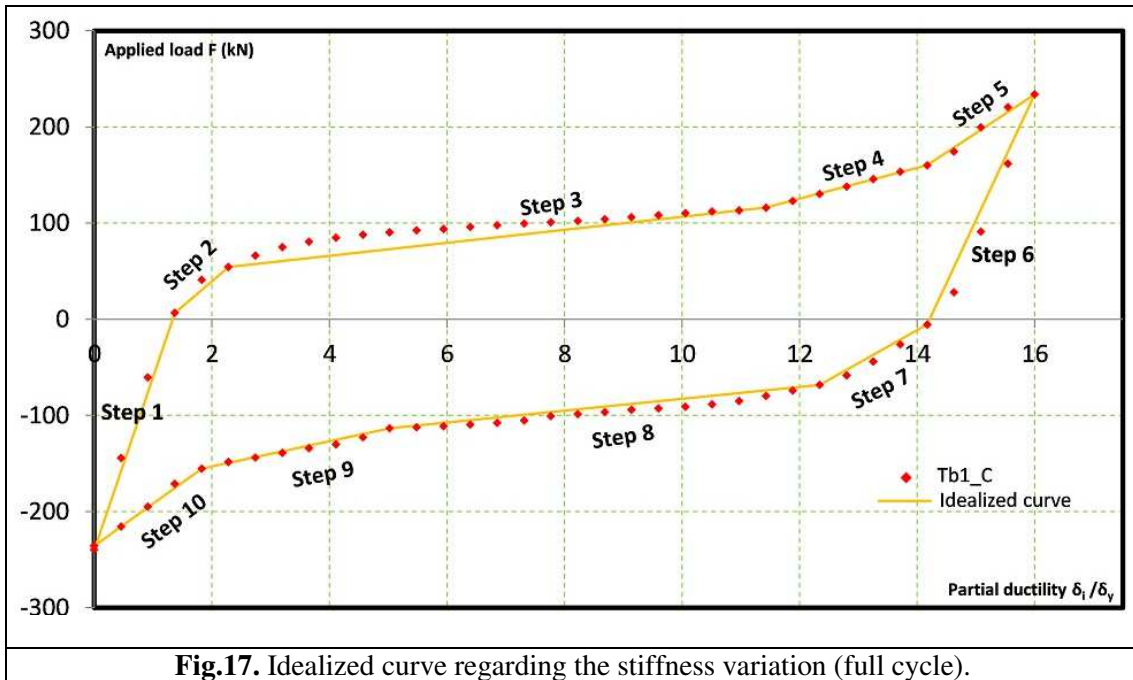
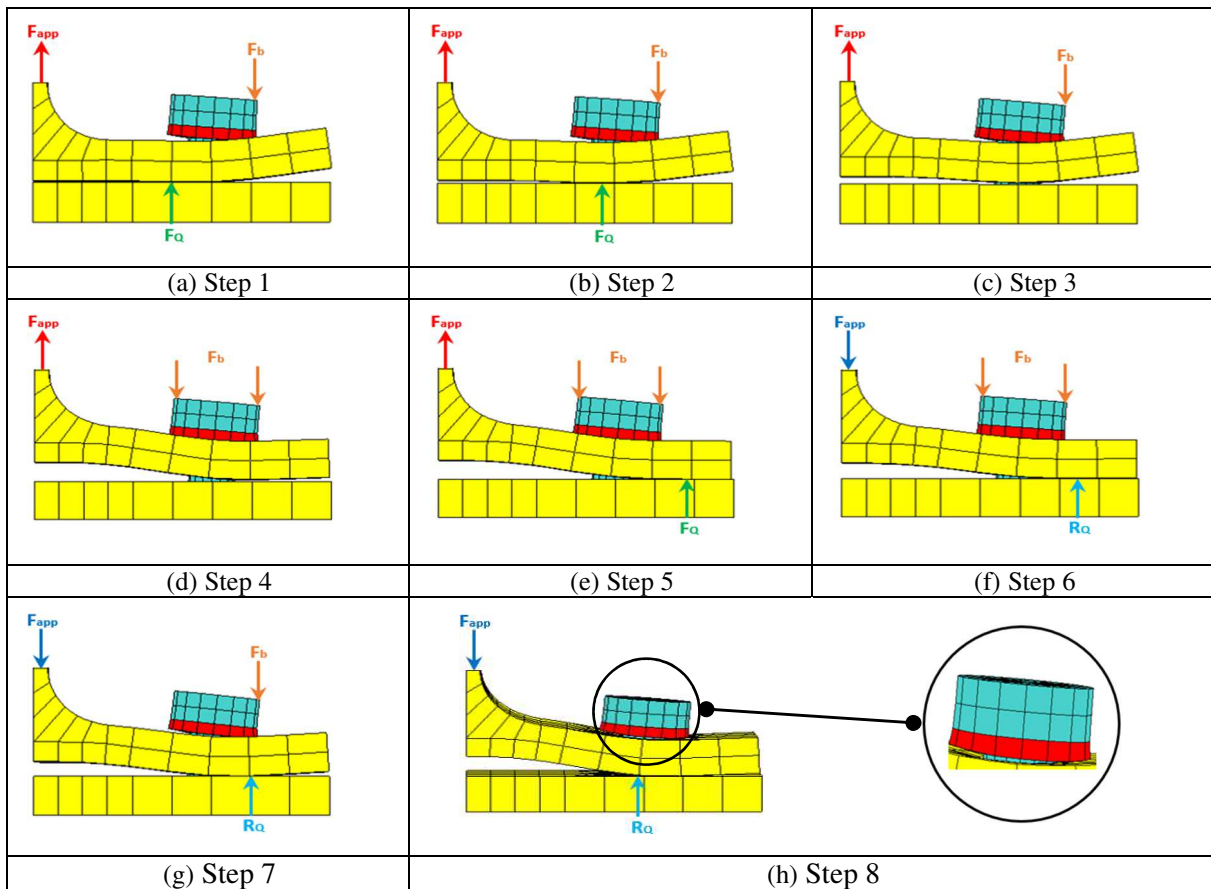
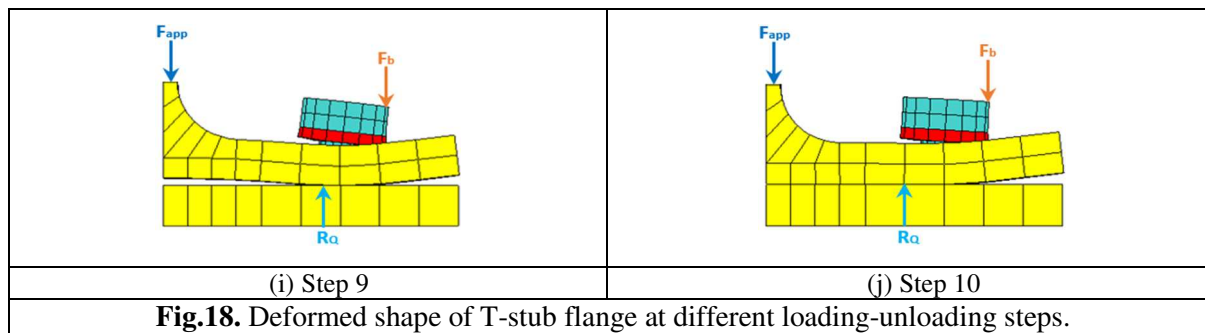


Fig.17. Idealized curve regarding the stiffness variation (full cycle).

296





**Fig.18.** Deformed shape of T-stub flange at different loading-unloading steps.

297

### 298 3.3.2. Key performance parameters

299 The performance of the T-stubs subjected to cyclic loads is evaluated by using the parameters defined  
 300 by the ECCS [38] such as the strength ratio, the resistance drop and the energy absorption, for each  
 301 loading cycle. These parameters are analyzed in function of the partial ductility  $\delta_i/\delta_y$  for displacement  
 302 values  $\delta_i > \delta_y$  [38] All T-stubs are subjected to repetitive cyclic loading with an imposed positive  
 303 displacement, due to their design and symmetry. Therefore, only the positive parameters are analyzed.

#### 304 a) Strength ratio

305 The ratio of the strength for each loading cycle at peak displacement (Fig. 19) to the initial yield  
 306 strength of the connections, given by the by the formula  $\epsilon_i^+ = F_i^+ / F_y^+$  is an important parameter that is  
 307 used to evaluate the performance of connections under dynamic/cyclic loadings that result from  
 308 earthquake ground motions [43]. Fig. 20 shows that there is a decrease in strength ratio for each group  
 309 of three cycles of equal displacement for all T-stubs ( $T_{b1c\_M12}$ ,  $T_{g1c\_M16}$ ,  $T_{b2c\_M12}$  and  $T_{g2c\_M16}$ ).  
 310 However, the strength ratios of T-stubs  $T_{b2c\_M12}$  and  $T_{g2c\_M16}$  are higher than those of T-stubs  $T_{b1c\_M12}$   
 311 and  $T_{g1c\_M16}$ . The strength ratios ( $\epsilon$ ) corresponding to the 28<sup>th</sup> cycle are given in Table 4. The ratio of  
 312 strength at peak displacement to the initial yield strength of T-stubs with two bolts is respectively 28%  
 313 and 44% for  $T_{b1c\_M12}$  and  $T_{g1c\_M16}$ . This ratio is higher of about 10% for T-stubs with four bolt rows  
 314 where it reaches 36% for  $T_{b2c\_M12}$  and 57% for  $T_{g2c\_M16}$ . It can be concluded that for each group of  
 315 three cycles of equal displacement, a higher strength ratio is obtained by the addition of an external  
 316 bolt row.

#### 317 b) Resistance drop ratio

318 The resistance drop ratio is equal to the ratio of the strength of the third cycle to that of the first cycle  
 319 as given by the following formula  $\epsilon^{+*} = F_i^+ / F_{i-2}^+$  where  $F_i$  and  $F_{i-2}$  represent respectively the external  
 320 force applied for cycle  $i$  (third cycle) and cycle  $i-2$  (first cycle) for each group of three cycles of equal  
 321 displacement (Fig. 21). The curves showing the variation of the resistance drop ratio as a function of  
 322 the partial ductility ( $\delta_i/\delta_y$ ) are given in Fig. 22. It can be seen than during the first two groups of three  
 323 cycles of equal displacement, the T-stubs with four bolts are characterized by an increase of the

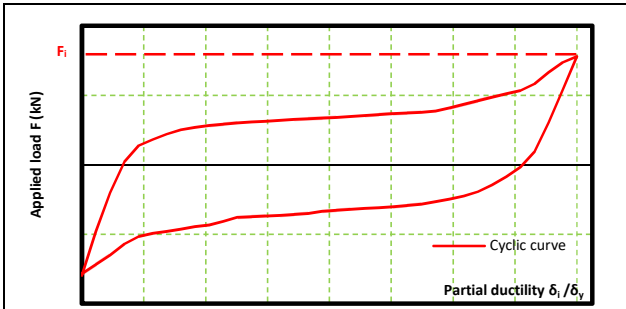
324 resistance drop ratio of about 7% ( $T_{b2c\_M12}$  and  $T_{g2c\_M16}$ ) whilst there is an increase of only around 4%  
 325 for the T-stubs with two bolts ( $T_{b1c\_M12}$  and  $T_{g1c\_M16}$ ). Following the first two groups of three cycles, a  
 326 decrease of about 5% in the strength drop ratio of two bolts row T-stubs is observed that is due to the  
 327 yielding of their plate. However, in the case of four bolts T-stubs, the strength of the third cycle is  
 328 almost equal to the strength of the first cycle (Table 4) and therefore practically no decrease in the  
 329 strength drop ratio is observed. This indicates that due to the external bolts, the T-stubs with four-bolt  
 330 are not affected by the repetition of the same loading cycle.

331 c) Absorbed energy

332 Connections subjected to cyclic loading must have the ability to absorb and dissipate energy in order  
 333 to guarantee the stability of the structure. This can be measured by the energy absorption capacity as a  
 334 function of the partial ductility ( $\delta_i/\delta_y$ ). This parameter is defined by the following formula:

335 
$$n_i^+ = A_i^+ / F_y^+ (\delta_i^+ - \delta_y^+ + \delta_i^- - \delta_y^-)$$

336 The curves giving the energy absorption capacity versus partial ductility are shown in Fig. 23 ( $\delta_i/\delta_y$ ). It  
 337 can be observed that there is greater energy absorption in the case of T-stubs  $T_{b2c\_M12}$  and  $T_{g2c\_M16}$  than  
 338 for T-stubs  $T_{b1c\_M12}$  and  $T_{g1c\_M16}$  for which it does not exceed the value of 0.66 whilst the values of  $n_i^+$   
 339 for T-stubs  $T_{b2c\_M12}$  and  $T_{g2c\_M16}$  corresponding to the 28<sup>th</sup> loading cycle reached 0.78 and 0.91  
 340 respectively (Table 4). It can be concluded from these results that there is higher energy absorption in  
 341 the case of the T-stubs with four bolts row than for the T-stubs with two bolts row.



342 **Fig. 19.** Determination of the value ( $F_i$ ) for cycle  $i$ .

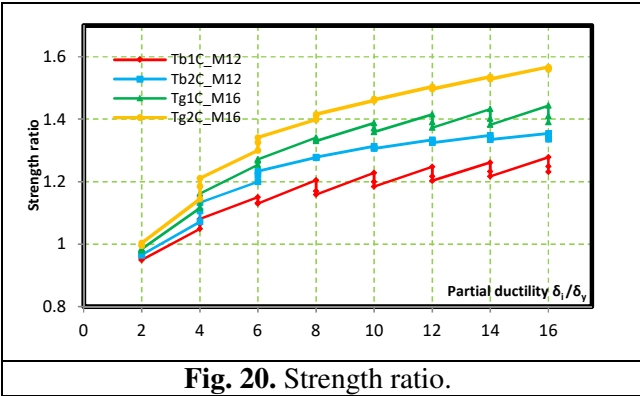


**Fig. 20.** Strength ratio.

343

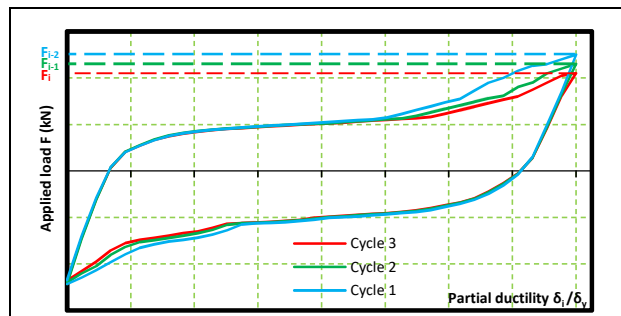


**Fig. 21.** Determination of the values ( $F_i$ ,  $F_{i-1}$  and  $F_{i-2}$ ) for cycles  $i$ ,  $i-1$  and  $i-2$ .

344

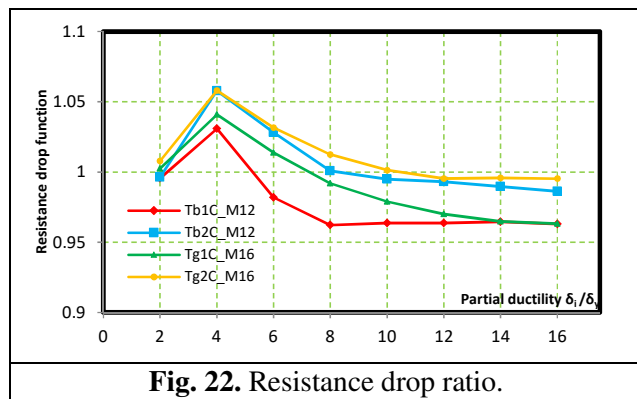


**Fig. 22.** Resistance drop ratio.

345

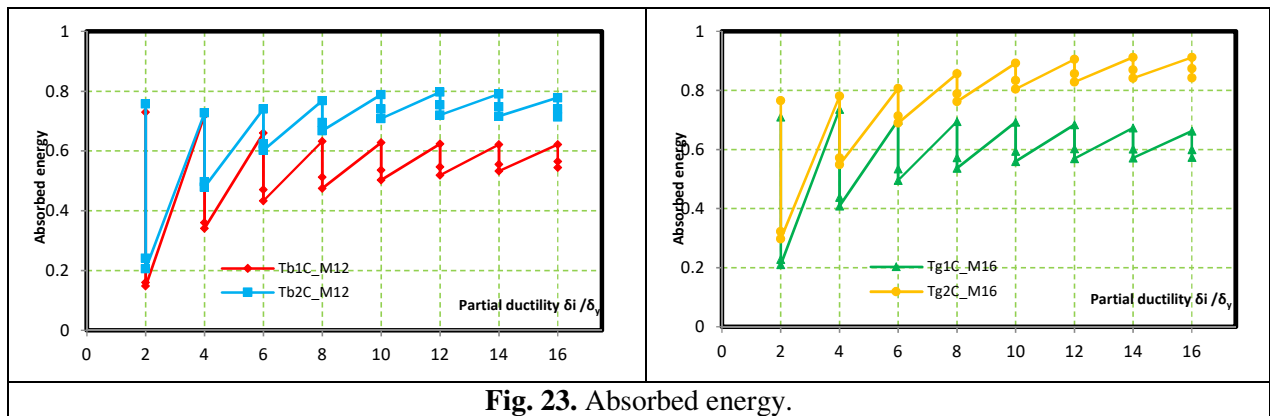


**Fig. 23.** Absorbed energy.

346

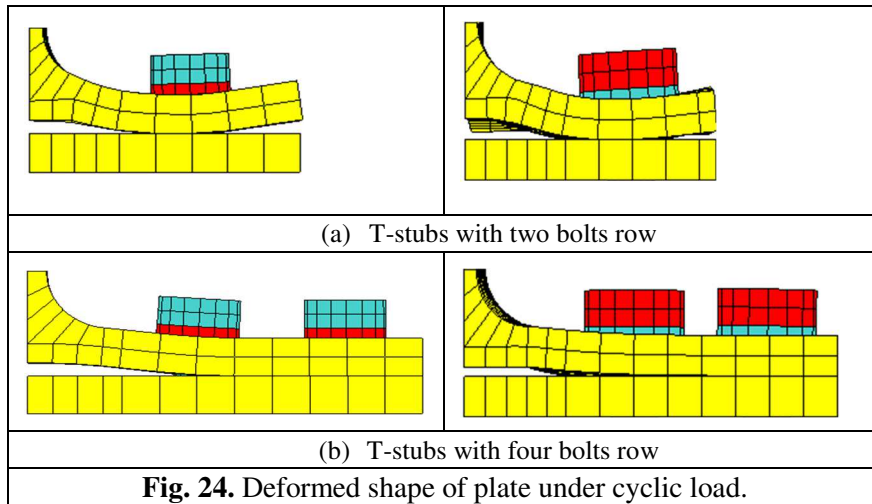
**Table 4**  
Key performance parameters.

T-stub	Tb1c_M12	Tb2c_M12	Tg1c_M16	Tg2c_M16
Strength ratio( $\epsilon$ )	1,28	1,36	1,44	1,57
Resistance drop fuction ( $\epsilon^*$ )	0,96	0,98	0,96	0,99
Absorbed energy ( $n_i$ )	0,62	0,78	0,66	0,91

347

348 3.3.3. Deformed shapes of T-stubs with two and four bolts rows

349 Fig. 24 shows that there is an uplift of the end part of the T-stubs plate with two bolts ( $T_{b1c\_M12}$  and  
 350  $T_{g1c\_M16}$ ) but no uplift is observed in the case of T-stubs with four bolts per row ( $T_{b2c\_M12}$  and  $T_{g2c\_M16}$ ).  
 351 Therefore, the addition of outer bolts prevents the end part of T-stub plate from lifting, thus  
 352 maintaining its contact with the foundation, avoiding the temporary cancellation of the prying forces  
 353 that corresponds to the decrease in the stiffness of the T-stubs.



354

#### 355 4. Analysis of the evolution of the Prying forces and the bolts behavior

##### 356 4.1. The Prying forces

357 The variations of the prying forces on the contact zone under the T-stub flange are plotted in Fig. 25  
 358 for all T-stubs. The FE results show that the shapes of the curves for the T-stubs with two bolts per  
 359 row are similar and are characterized by the temporary disappearance of the prying forces during the  
 360 loading phase (Fig. 25) due to the loss of the contact between the plate and the foundation (Fig. 18c).  
 361 As far as T-stubs with four bolts per row ( $T_{b2c\_M12}$  and  $T_{g2c\_M16}$ ) are concerned, no cancellation of the  
 362 prying forces occurs although the curves showing the evolution of the prying forces versus the applied  
 363 load are similar to those of the T-stubs with two bolts. This is because the plate stays flat (Fig. 24b),  
 364 thus preventing its loss of contact with the foundation. Furthermore, it can be observed during the  
 365 unloading phase that compressive forces develop under the plate of all T-stubs instead of the usual  
 366 prying forces. However, the compressive forces present in the case of the four bolts row T-stubs have  
 367 greater values than those of the T-stubs with two-bolt row. This is due to the higher resistance of the  
 368 four-bolt row T-stubs when compared to those with two-bolts row. The prying forces are plotted  
 369 versus the applied force during the last cycle (4, 16 and 28<sup>th</sup> cycle) of each zone (Fig. 26). In zone I  
 370 (Fig. 26a), it can be observed that the curves are linear for the all T-stubs ( $T_{b1c\_M12}$ ,  $T_{g1c\_M16}$ ,  $T_{b2c\_M12}$   
 371 and  $T_{g2c\_M16}$ ), with slightly higher values of the prying forces for the T-stubs with four bolts ( $T_{b2c\_M12}$   
 372 and  $T_{g2c\_M16}$ ). In zones II and III (Figs. 26b and c), during the loading phase, due to the total contact  
 373 loss between the plate and the foundation, temporary cancellation of the prying forces of the T-stubs

374 with two-bolt is observed. This cancellation is more significant in zone III (Fig. 26c), due to the more  
 375 pronounced yielding of the plate. However, in the case of T-stubs with four bolts, the prying forces are  
 376 mobilized continuously. During the unloading phase, as previously explained, the prying forces are  
 377 replaced by compression forces under the plate, these forces being about 10% greater in zone II and  
 378 about 20% in zone III for the T-stubs with four bolts ( $T_{b2c\_M12}$  and  $T_{g2c\_M16}$ ) compared to the T-stubs  
 379 with two bolts ( $T_{b1c\_M12}$  and  $T_{g1c\_M16}$ ).

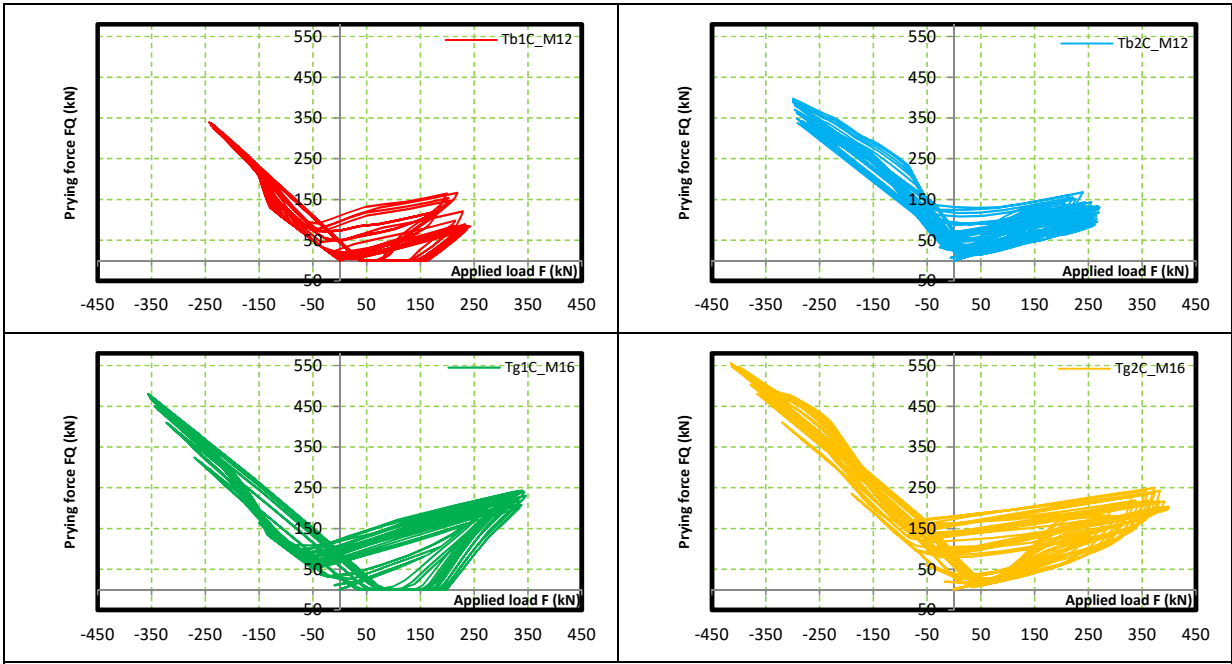
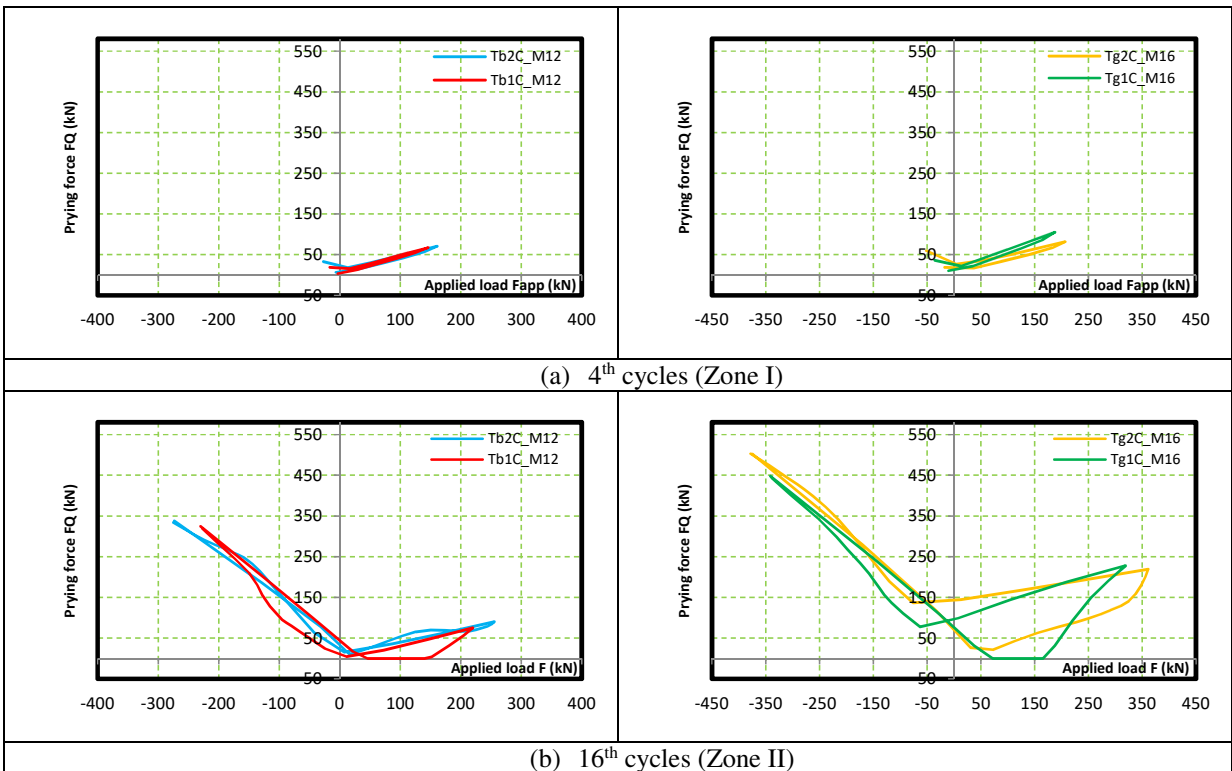
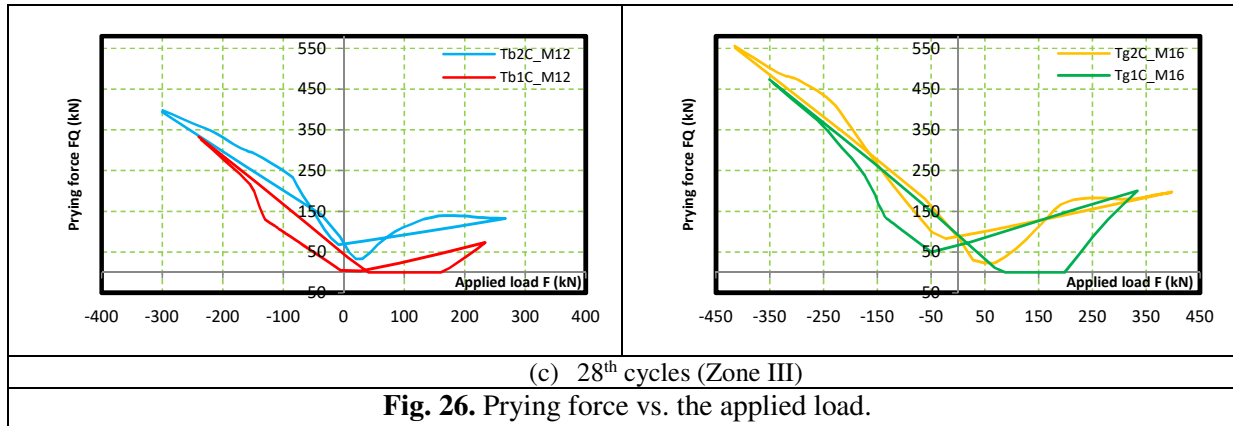


Fig. 25. Prying force vs. the applied load.

380





381

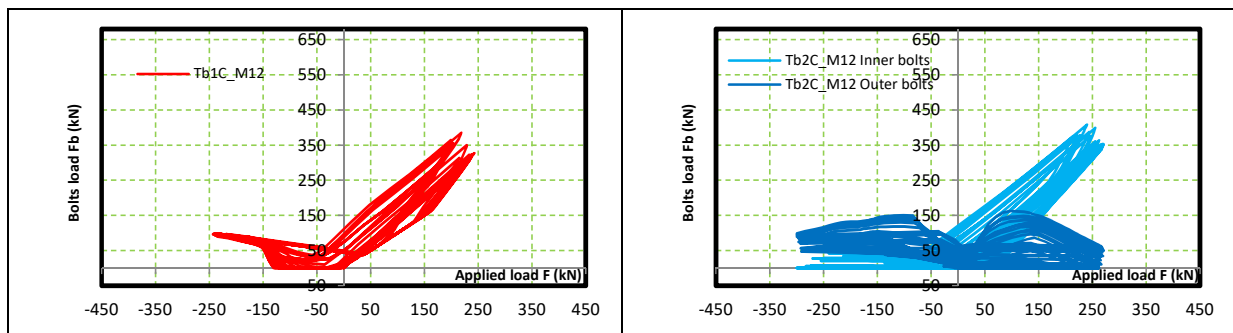
382 4.2. Analysis of the Bolts behavior

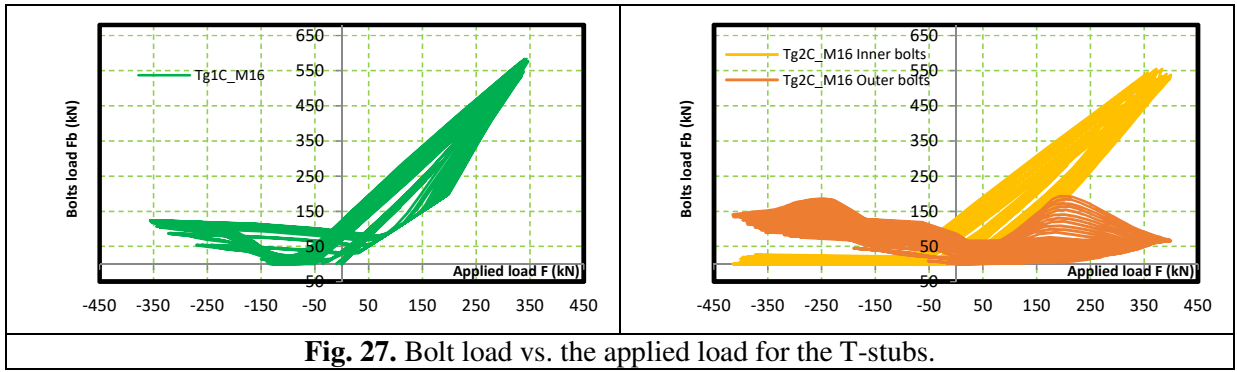
383 The forces in the bolts of T-stubs with two bolts ( $T_{b1c\_M12}$  and  $T_{g1c\_M16}$ ) and those of the inner and outer  
 384 bolts of T-stubs with four bolts ( $T_{b2c\_M12}$  and  $T_{g2c\_M16}$ ) are plotted versus the applied load in Fig. 27.  
 385 During the loading phase, the behavior of the bolts of the T-stubs  $T_{b1c\_M12}$  and  $T_{g1c\_M16}$  is similar to that  
 386 of the inner bolts of the T-stubs  $T_{b2c\_M12}$  and  $T_{g2c\_M16}$ . However, during the unloading phase, the inner  
 387 bolts of T-stubs  $T_{b2c\_M12}$  and  $T_{g2c\_M16}$  are unloaded in contrast with those of T-stubs  $T_{b1c\_M12}$  and  
 388  $T_{g1c\_M16}$ , where the participation of the bolts in the resistance to the applied load is only cancelled  
 389 temporarily because of the contact loss between the head of the bolts and the plate (Fig. 18h). As  
 390 regards the outer bolts of T-stubs  $T_{b2c\_M12}$  and  $T_{g2c\_M16}$ , in addition to their contribution to the resistance  
 391 of the applied load during the loading phase, they also participate to the resistance during the  
 392 unloading phase, thus compensating for the fact that the internal bolts play no role during the  
 393 unloading phase. This ensures that the bolts contribute to the strength of T-stubs during the loading  
 394 and unloading phases. Values of the forces in the bolts of T-stubs with two and four bolts per row are  
 395 plotted as a function of applied force for the last cycle (4, 16, and 28 cycles) of each Zone (Fig. 28).  
 396 The contributions from the bolts of T-stubs  $T_{b1c\_M12}$  and  $T_{g1c\_M16}$  ( $F_b$ ) and from the inner ( $F_{bi}$ ) and outer  
 397 ( $F_{bo}$ ) bolts of the T-stubs  $T_{b2c\_M12}$  and  $T_{g2c\_M16}$  during the loading and unloading phases for the 4<sup>th</sup>, 16<sup>th</sup>  
 398 and 28<sup>th</sup> cycle are given in Tables 5 and 6. The values given correspond to the maximum value of the  
 399 applied load during loading and unloading. In zones I and II (Figs. 28a and b) a similar variation in the  
 400 forces in the bolts of T-stubs with two bolts and the inner bolts of the T-stubs with four bolts is  
 401 observed during the loading phase. At the end of the first zone, each of these bolts is subjected to an  
 402 axial force of around 55kN for T-stubs  $T_{b1c\_M12}$  and  $T_{b2c\_M12}$ , and an axial force of around 70kN for T-  
 403 stubs  $T_{g1c\_M16}$  and  $T_{g2c\_M16}$ . As regards zone II, for T-stubs with two bolts per row, each bolt of  
 404  $T_{b1c\_M12}$  and  $T_{g1c\_M16}$  is subjected to axial forces whose values are equal to about 75kN and 135kN  
 405 respectively. In the case of T-stubs with four bolts, in this second zone, the axial force measured in  
 406 each inner bolt of  $T_{b2c\_M12}$  and  $T_{g2c\_M16}$  is equal to around 85kN and about 130kN respectively. In the  
 407 case of the outer bolts, no contribution to the resistance is observed in zone I (Fig. 28a). However, in

408 Zone II, a slight contribution to the applied load is observed (Fig. 28b). During the unloading phase in  
 409 Zones I and II (Figs. 28a and b), the contribution of the bolts of T-stub  $T_{b1c\_M12}$  to the resistance of the  
 410 T-stub is nil in Zone I and is cancelled temporarily in Zone II, after this cancellation each of the bolts  
 411 is subjected to an axial force of 23kN. Nevertheless, the contribution of the bolts to the resistance of T-  
 412 stub  $T_{g1c\_M16}$  is not cancelled in zone II (Fig. 28b), due to their higher strength, an axial load equal to  
 413 26kN being obtained from the FEM in every bolt of  $T_{g1c\_M16}$ . As regards T-stubs  $T_{b2c\_M12}$  and  $T_{g2c\_M16}$ ,  
 414 the inner bolts play practically no role in the resistance to the applied load in Zone II. However, the  
 415 outer bolts take up a substantial proportion of the applied load, thus compensating for the inner bolts.  
 416 In zone III (Fig. 28c), the contribution of T-stubs  $T_{b1c\_M12}$  and  $T_{g1c\_M16}$  bolts to the resistance of the  
 417 applied load is similar during the loading and unloading phase. This contribution is characterized, by a  
 418 temporary cancellation of their participation to the resistance of the applied load in unloading phase.  
 419 This is due to the total contact loss between the head of the bolts and the plate. **Regarding the T-stubs**  
 420  **$T_{b2c\_M12}$  and  $T_{g2c\_M16}$ , the inner bolts do not contribute to the resistance at the start of loading and**  
 421 **during the unloading phase due to the contact loss with the plate. Nevertheless, in the loading**  
 422 **phase, when the applied load reaches about 50kN, the inner bolts start to participate to the**  
 423 **resistance of the T-stub owing to the plate uplift on the fillet radius side that restores the contact**  
 424 **between the head of the inner bolts and the plate.** However, that is not the case of the outer bolts  
 425 that contribute continuously to the resistance of the applied load during the loading and unloading  
 426 phase, thus compensating for the lack of contribution of the inner bolts during the loading and  
 427 unloading phase. It should be noted that both equilibrium Eqs. (2 and 3) are satisfied in the loading  
 428 and unloading phase when considering the forces obtained from the numerical model.

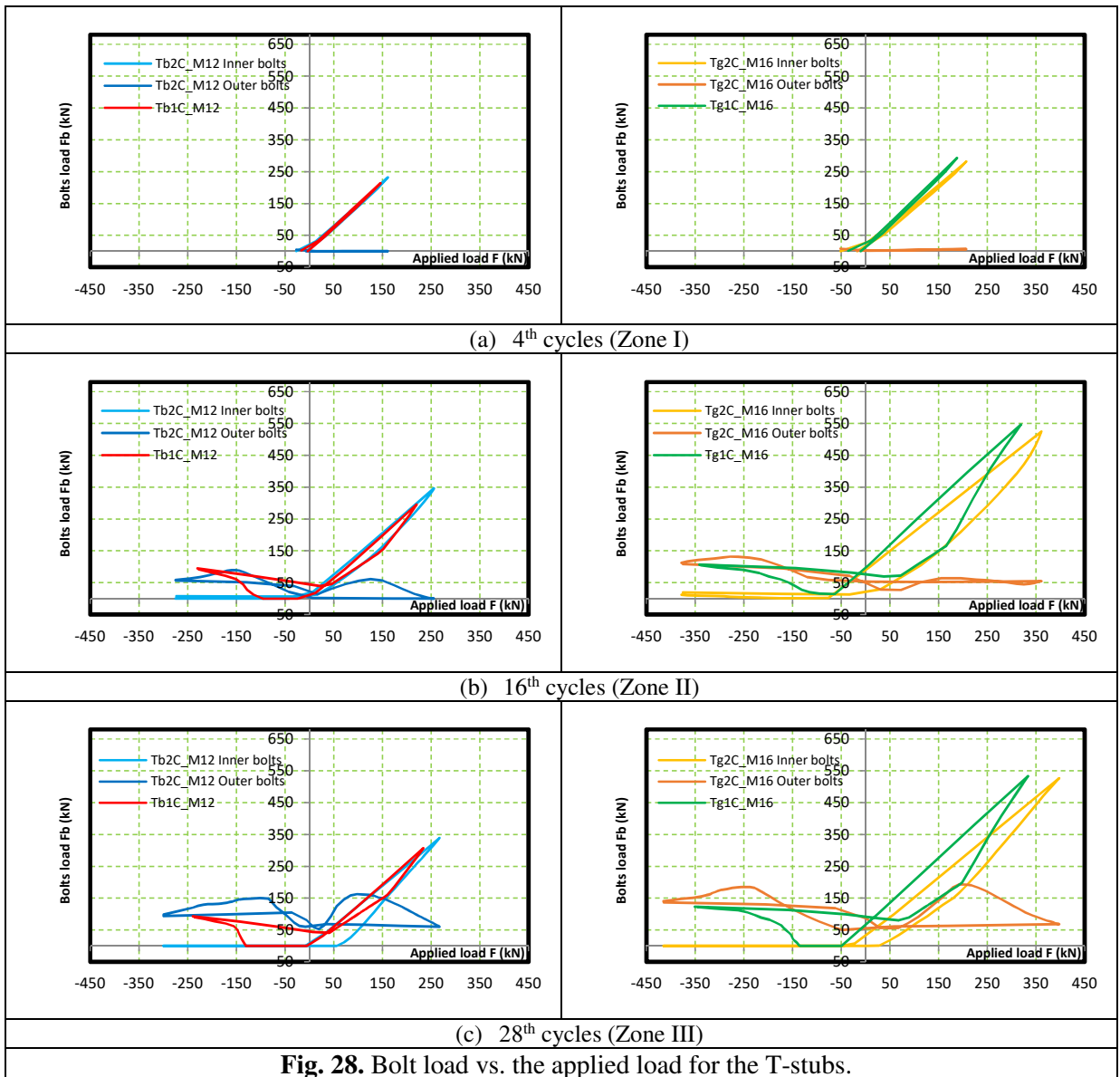
429  $F$  +  $F_Q$  =  $\sum F_b$   
 430 (2)

431  $F + R_Q = \sum F_b$  (3)





432



433

**Table 5**

Numerical values of prying forces and bolt forces during the loading phase for the last cycle of each Zone (4<sup>th</sup>, 16<sup>th</sup>, and 28<sup>th</sup>).

	Loading phase											
	4 <sup>th</sup> cycle				16 <sup>th</sup> cycle				28 <sup>th</sup> cycle			
	T <sub>b1c_M12</sub>	T <sub>b2c_M12</sub>	T <sub>g1c_M16</sub>	T <sub>g2c_M16</sub>	T <sub>b1c_M12</sub>	T <sub>b2c_M12</sub>	T <sub>g1c_M16</sub>	T <sub>g2c_M16</sub>	T <sub>b1c_M12</sub>	T <sub>b2c_M12</sub>	T <sub>g1c_M16</sub>	T <sub>g2c_M16</sub>
F (kN)	146	161	188	207	220	256	319	361	234	267	334	398
F <sub>bX4</sub> (kN)	214	/	293	/	296	/	547	/	307	/	533	/
F <sub>biX4</sub> (kN)	/	232	/	282	/	346	/	525	/	339	/	527
F <sub>boX4</sub> (kN)	/	0	/	0	/	0	/	55	/	61	/	68
F <sub>Q</sub> (kN)	68	70	105	75	76	90	228	219	73	133	199	197

434

**Table 6**

Numerical values of compressive forces and bolt forces during the unloading phase for the last cycle of each Zone (4<sup>th</sup>, 16<sup>th</sup>, and 28<sup>th</sup>).

	Unloading phase											
	4 <sup>th</sup> cycle				16 <sup>th</sup> cycle				28 <sup>th</sup> cycle			
	T <sub>b1c_M12</sub>	T <sub>b2c_M12</sub>	T <sub>g1c_M16</sub>	T <sub>g2c_M16</sub>	T <sub>b1c_M12</sub>	T <sub>b2c_M12</sub>	T <sub>g1c_M16</sub>	T <sub>g2c_M16</sub>	T <sub>b1c_M12</sub>	T <sub>b2c_M12</sub>	T <sub>g1c_M16</sub>	T <sub>g2c_M16</sub>
F (kN)	-16	-27	-36	-52	-227	-275	-339	-378	-236	-299	-344	-415
F <sub>bX4</sub> (kN)	3	/	1	/	92	/	105	/	90	/	122	/
F <sub>biX4</sub> (kN)	/	1	/	3	/	1	/	12	/	0	/	0
F <sub>boX4</sub> (kN)	/	5	/	8	/	58	/	113	/	99	/	141
R <sub>Q</sub> (kN)	13	21	35	41	168	216	234	253	146	200	122	247

435 4.3. Analysis of the bolts elongation

436 The elongations of the bolts of T-stub T<sub>b1c\_M12</sub> and those of the inner bolts of T-stub T<sub>b2c\_M12</sub> are  
437 compared in Fig. 29. During the loading phase, this elongation is minimal and equal for both T<sub>b1c\_M12</sub>  
438 bolts and T<sub>b2c\_M12</sub> inner bolts, until the applied load reaches its elastic limit value F<sub>y</sub> corresponding to  
439 180kN for the T-stub T<sub>b1c\_M12</sub> and 190kN for the T-stub T<sub>b2c\_M12</sub>. For loads greater than F<sub>y</sub>, there is a  
440 sharp increase in the value of the elongations of the bolts, this increase being higher in the case of  
441 T<sub>b1c\_M12</sub> bolts with an elongation equal to 4mm during the last cycle of zone III (28<sup>th</sup> cycle), that  
442 corresponds to an applied load equal to 230kN. However, at the same loading stage (28<sup>th</sup> cycle)  
443 corresponding to an applied load equal to 267kN the elongation of T<sub>b2c\_M12</sub> inner bolts, does not exceed  
444 3mm. The same findings are observed during the unloading phase. Therefore, there is a reduction of  
445 the elongation of the bolts when an outer row of bolts is added.

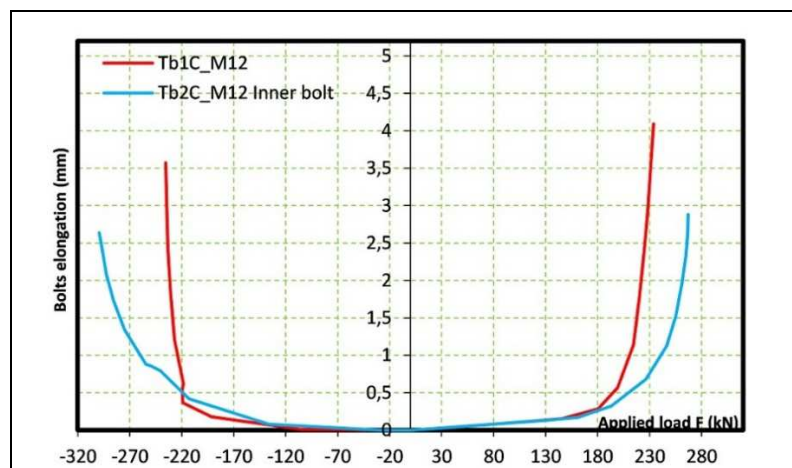


**Fig. 29. Bolts elongation.**

446

## 447 **5. Conclusion**

448 The study carried out in this paper compared the monotonic and cyclic behaviors of T-stubs with two  
449 and four bolts per row. Its main aim was to highlight the benefits of adding the outer bolts on the  
450 cyclic behavior of the T-stubs in comparison to that of two bolts row T-stubs. The comparison was  
451 based on the final deformation of the T-stub at the end of the loading cycles as well as the key  
452 parameters given by the ECCS recommendations [38]. The main results of the work can be  
453 summarized as follows:

- 454 • Under monotonic loads, the addition of an outer bolt has no significant impact until the flange  
455 starts to yield.
- 456 • **Under cyclic loads, the addition of an external row of bolts prevents the variation and  
457 the decrease of the stiffness as well as providing an increase in strength that can reach  
458 more than 80%.**
- 459 • Under cyclic loading, the outer bolts take up practically all of the load applied in the  
460 unloading phase, as well as participating to the resistance to the applied load in the loading  
461 phase.
- 462 • **The addition of the outer bolts prevents the uplift of the end part of the T-stub plate  
463 subjected to the cyclic loads, thus avoiding the cancellation of the prying forces, as well  
464 as reducing the elongation of the inner bolts of about 40% in the loading and unloading  
465 phase.**

466 **Furthermore, the analysis of the key parameters given by the ECCS [38] showed that the  
467 repetition of the same loading cycle with an equal displacement had a great influence on the  
468 behavior of the T-stubs with two bolts and will result in a large loss of strength. However, this  
469 loss has been reduced of about 10% by the addition of an external row of bolts. Also, the analysis  
470 of these key parameters showed that due to the stability of the hysteresis loops, the four-bolt T-  
471 stubs absorb around 20% more energy than the two-bolt T-stubs**

472 **Finally, the results presented in this paper are promising with regard to the improvement of  
473 the cyclical behavior of the two-bolt T-stubs, particularly the strength ratio and the energy  
474 absorption capacity. Detailed investigations of the deformations and evolution of bolt loads  
475 along with contact pressures provided an understanding of the mechanical behavior of the T-  
476 stubs with 2 and 4 bolts under cyclic loading. The description of the evolution of stiffness during  
477 a full cycle will allow the development of an analytical model.**

478           **Consequently, the upcoming research activity of the authors will aim at the development of**  
479 **an analytical model based on both the component method and the previous studies that were**  
480 **carried out by Piluso and Rizzano [3]. This model will be developed with the purpose of**  
481 **characterizing the actual hysterical behavior of two-bolt and four-bolt T-stubs, considering their**  
482 **mechanical and geometrical characteristics and also the different degradations.**

### 483 **Acknowledgments**

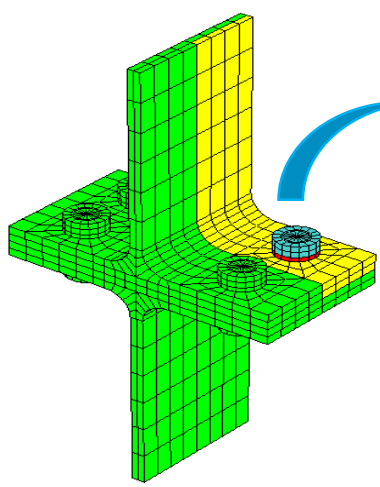
484 The authors wish to thank Algerian and French governments as well as the DGRSDT for the financial  
485 support provided through the cooperation project Profas B+ 2019.

### 486 **References**

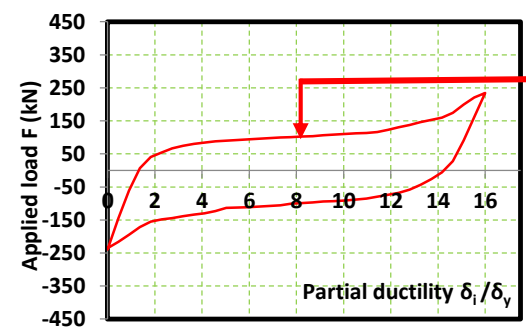
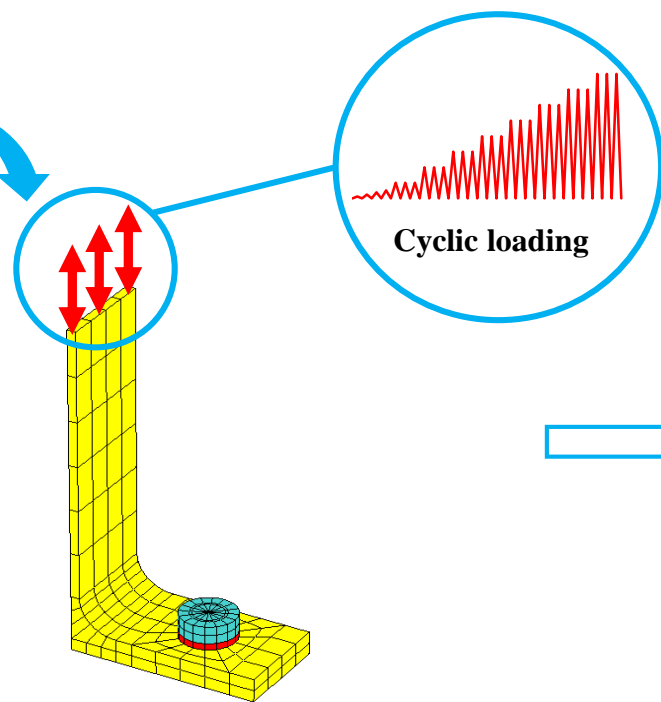
- 487 [1] FEMA, FEMA 355E State of the Art Report on Past Performance of Steel Moment-frame  
488 Buildings in Earthquakes, Washington DC, USA, Federal Emergency Management Agency,  
489 2000.
- 490 [2] D. Grecea, F. Dinu, D. Dubina, Performance criteria for MR steel frames in seismic zones, J.  
491 Constr. Steel Res. 2004 60:739-749. [https://doi.org/10.1016/S0143-974X\(03\)00140-8](https://doi.org/10.1016/S0143-974X(03)00140-8).
- 492 [3] V. Piluso, G. Rizzano, Experimental analysis and modelling of bolted T-stubs under cyclic loads,  
493 J. Constr. Steel Res. 64 (2008) 655-669. <https://doi.org/10.1016/j.jcsr.2007.12.009>.
- 494 [4] R. Herrera, C. Salas, J.F. Beltran, E. Nuñez, Experimental performance of double built-up T  
495 moment connections under cyclic loading, J. Constr. Steel Res. 138 (2017) 742-749.  
496 <https://doi.org/10.1016/j.jcsr.2017.08.022>.
- 497 [5] S. El-Khoriby, M.A. Sakr, T.M. Khalifa, M.M. Eladly, Modelling and behaviour of beam-to-  
498 column connections under axial force and cyclic bending, J. Constr. Steel Res. 129 (2017)171-  
499 184. <https://doi.org/10.1016/j.jcsr.2016.11.006>.
- 500 [6] SAC. Analytical and field investigations of buildings affected by the northridge earthquake of  
501 january 17,1994. Sacramento, California, 1995.
- 502 [7] E.A. Sumner, T. Murray, Behavior of extended end-plate moment connections subject to cyclic  
503 loading, J. Struct. Eng. 128 (2002) 501-508.
- 504 [8] A. Lemos, L. Simões da Silva, M. Latour, G. Rizzano, Numerical modelling of innovative DST  
505 steel joint under cyclic loading, Arch. Civil. Mech. Eng. 18 (2018) 687-701.  
506 <https://doi.org/10.1016/j.a.cme.2017.10.008>.
- 507 [9] Z. Al-Khatib, A. Bouchaïr, Analysis of a bolted T-stub strengthened by backing-plates with regard  
508 to Eurocode 3, J. Constr. Steel Res. 63 (2007) 1603-1615. <https://doi.org/10.1016/j.jcsr.2007.01.012>.
- 509
- 510 [10] A. Bouchaïr, J. Averseng, A. Abidelah, Analysis of the behaviour of stainless steel bolted  
511 connections, J. Constr. Steel Res. 64 (2008) 1264–1274. <https://doi.org/10.1016/j.jcsr.2008.07.009>.
- 512
- 513 [11] A. Abidelah, A. Bouchaïr, D. Kerdal, Influence of the flexural rigidity of the bolt on the behavior  
514 of the T-stub steel connection, Eng. Struct. 81 (2014) 181-194. <https://doi.org/10.1016/j.engstruct.2014.09.041>.
- 515
- 516 [12] A.B. Francavilla, M. Latour, V. Piluso, G. Rizzano, Simplified finite element analysis of bolted  
517 T-stub connection components, Eng. Struct. 100 (2015) 656-664.  
518 <https://doi.org/10.1016/j.engstruct.2015.06.029>.
- 519 [13] Z. Kong, S.E. Kim, Numerical estimation for initial stiffness and ultimate moment of T-stub  
520 connections, J. Constr. Steel Res. 141 (2018) 118-131. <https://doi.org/10.1016/j.jcsr.2017.11.008>.

- 521 [14] L. Gödrich, F. Wald, J. Kabeláč, M. Kuříková, Design finite element model of a bolted T-stub  
522 connection component, *J. Constr. Steel Res.* 157 (2019) 198-206. <https://doi.org/10.1016/j.jcsr.2019.02.031>.  
523
- 524 [15] L.M. Bezerra, J. Bonilla, W.A. Silva, W.T. Matias, Experimental and numerical studies of bolted  
525 T-stub steel connection with different flange thicknesses connected to a rigid base, *Eng. Struct.*  
526 (2020) 218. <https://doi.org/10.1016/j.engstruct.2020.110770>.
- 527 [16] CEN, Eurocode 3: Design of steel structures-Part 1-8: Design of joints. Brussels, 2005.
- 528 [17] H. Augusto, L. Simões da Silva, C. Rebelo, J.M. Castro, Cyclic behaviour characterization of web  
529 panel components in bolted end-plate steel joints, *J. Constr. Steel Res.* 133 (2017) 310-333.  
530 <https://doi.org/10.1016/j.jcsr.2017.01.021>.
- 531 [18] C. Bernuzzi, R. Zandonini, P. Zanon, Experimental analysis and modelling of semi-rigid steel  
532 joints under cyclic reversal loading, *J. Constr. Steel Res.* 38 (1996) 95-123.  
533 [https://doi.org/10.1016/0143-974X\(96\)00013-2](https://doi.org/10.1016/0143-974X(96)00013-2).
- 534 [19] N. Nemati, D. Le Houedec, R. Zandonini, Numerical modelling of the cyclic behaviour of the  
535 basic components of steel end plate connections, *Advances. Eng. Software.* 31 (2000) 837-847.  
536 [https://doi.org/10.1016/S0965-9978\(00\)00046-6](https://doi.org/10.1016/S0965-9978(00)00046-6).
- 537 [20] M. Gerami, H. Saberi, V. Saberi, A.S. Daryan, Cyclic behavior of bolted connections with  
538 different arrangement of bolts, *J. Constr. Steel Res.* 67 (2011) 690-705.  
539 <https://doi.org/10.1016/j.jcsr.2010.11.011>.
- 540 [21] M. Latour, P. Piluso, R. Rizzano, Cyclic modeling of bolted beam-to-column connections:  
541 component approach, *J. Earthq. Eng.* 15 (2011) 537-563. <http://dx.doi.org/10.1080/13632469.2010.513423>.  
542
- 543 [22] F. Iannone, M. Latour, V. Piluso, G. Rizzano, Experimental Analysis of Bolted Steel Beam-to-  
544 Column Connections: Component Identification, *J. Earthq. Eng.* 15 (2011) 214-244.  
545 <https://doi.org/10.1080/13632461003695353>.
- 546 [23] L. Simões da Silva, A. Shahbazian, F. Gentili, H. Augusto, "Implementation of a component  
547 model for the cyclic behaviour of steel joints", Proceedings of Eighth International Workshop on  
548 Connection in Steel Structures, Boston, USA, 2016 153-162.
- 549 [24] A. ElSabbagh, T. Sharaf, S. Nagy, M. ElGhandour, Behavior of extended end-plate bolted  
550 connections subjected to monotonic and cyclic loads, *Eng. Struct.* 190 (2019) 142-159.  
551 <https://doi.org/10.1016/j.engstruct.2019.04.016>.
- 552 [25] A. Ghobarah, A. Osman, R.M. Korol, Behaviour of extended end-plate connections under cyclic  
553 loading, *Eng. Struct.* 12 (1990)15-27. [https://doi.org/10.1016/0141-0296\(90\)90034-P](https://doi.org/10.1016/0141-0296(90)90034-P).
- 554 [26] A. Abidelah, A. Bouchaïr, D. Kerdal, Experimental and analytical behavior of bolted end-plate  
555 connections with or without stiffeners, *J. Constr. Steel Res.* 76 (2012) 13-27. <https://doi.org/10.1016/j.jcsr.2012.04.004>.  
556
- 557 [27] J.F. Demonceau, J.P. Jaspart, K. Weynand, R. Oerder, C. Muller, "Connections with four bolts  
558 per horizontal row", In: Proc Eurosteel, Budapest, Hungary, 2011.
- 559 [28] R. Tartaglia, M. D'Aniello, G.A. Rassati, J.A. Swanson, R. Landolfo, Full strength extended  
560 stiffened end-plate joints: AISC vs recent European design criteria, *Eng. Struct.* 159 (2018)155-  
561 171. <https://doi.org/10.1016/j.engstruct.2017.12.053>.
- 562 [29] S.N. El Kalash, E.G. Hantouche, Prying effect in unstiffened extended endplate connection with  
563 circular bolts configuration, *J. Const. Steel Res.* 160 (2019) 402-410. <https://doi.org/10.1016/j.jcsr.2019.05.043>.  
564
- 565 [30] CEN, Eurocode 8: Design of structures for earthquake resistance -Part 1: General rules, seismic  
566 actions and rules for buildings. Brussels, 2005.
- 567 [31] A. Kozłowski, Z. Pisarek, Resistance and stiffness of T-stub with four bolts, *Arch. Civ. Eng.*  
568 (2008)167-191.
- 569 [32] J.F. Demonceau, K. Weynand, J.P. Jaspart, C. Müller, "Application of Eurocode 3 to steel  
570 connections with four bolts per horizontal row", Proceedings Stability and Ductility of Steel  
571 Structures, Rio de Janeiro, Brazil, 2010 199-206.

- 572 [33] M. Latour, G. Rizzano, A. Santiago, L. Simões da Silva, Experimental analysis and mechanical  
573 modeling of T-stubs with four bolts per row, *J. Const. Steel Res.*101 (2014)158–174.  
574 <https://doi.org/10.1016/j.jcsr.2014.05.004>.
- 575 [34] S. Haouas, A. Abidelah, D. Kerdal, A. Bouchaïr, The mechanical behaviour of T-stubs with four  
576 bolts per row, *Proc. Inst. Civ. Eng.* 172 (2019) 882–901. <https://doi.org/10.1680/jstbu.18.00055>.
- 577 [35] CEA (Commissariat à l’Energie Atomique, France) CAST3M 2017 “CAST3M Website”, [http://w](http://www-cast3m.cea.fr)  
578 [ww-cast3m.cea.fr](http://www-cast3m.cea.fr).
- 579 [36] O.S. Bursi, J.P. Jaspart, Basic issues in the finite element simulation of extended end plate  
580 connections, *Comput and Struct.* 69 (1998) 361-382. [https://doi.org/10.1016/S0045-](https://doi.org/10.1016/S0045-7949(98)00136-9)  
581 [7949\(98\)00136-9](https://doi.org/10.1016/S0045-7949(98)00136-9).
- 582 [37] N. Gebbeken, H. Rothert, B. Binder, On the numerical analysis of endplate connections, *J.*  
583 *Constr. Steel Res.* 30 (1994) 177-196. [https://doi.org/10.1016/0143-974X\(94\)90049-3](https://doi.org/10.1016/0143-974X(94)90049-3).
- 584 [38] ECCS, Technical Committee 1: structural safety and loadings: technical working group 1.3:  
585 seismic design, recommended testing procedure for assessing the behaviour of structural steel  
586 elements under cyclic loads, 1986.
- 587 [39] Alkhatib Z, “Analysis of the behaviour of steel joints strengthened by backingplates-Numerical  
588 approach and experimental calibration”. PhD thesis, Blaise Pascal University, Clermont 2,  
589 France, 2003 (in French).
- 590 [40] A. Abidelah, “Numerical analysis of the behavior of steel connection approach and experimental  
591 calibration”. PhD thesis. Blaise Pascal University, Clermont 2, France, 2009 (in French).
- 592 [41] O.S. Bursi, J.P. Jaspart, Calibration of a finite element model for isolated bolted end-plate steel  
593 connections, *J. Constr. Steel Res.* 44 (1997) 225-262. [https://doi.org/10.1016/S0143-](https://doi.org/10.1016/S0143-974X(97)00056-4)  
594 [974X\(97\)00056-4](https://doi.org/10.1016/S0143-974X(97)00056-4).
- 595 [42] H. Agerskov, High-Strength Bolted Connections Subject to Prying, *J. Struct. Div.*102 (1976)161-  
596 175.
- 597 [43] W. Tizani, Z.Y. Wang, I. Hajirasouliha, Hysteretic performance of a new blind bolted connection  
598 to concrete filled columns under cyclic loading: An experimental investigation, *Eng. Struct.* 46  
599 (2013) 535-546. <http://dx.doi.org/10.1016/j.engstruct.2012.08.020>.

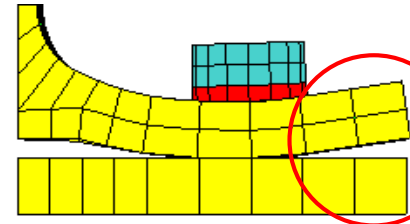


**T-stub with 2 bolts**



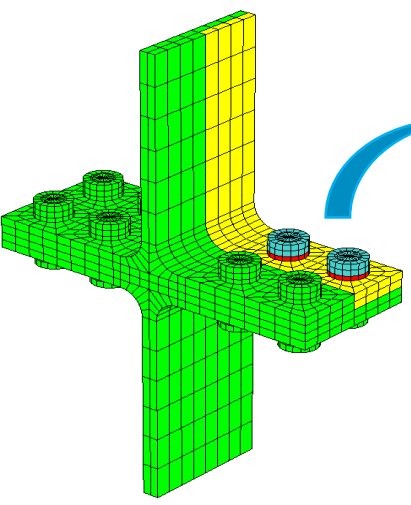
**Significant decrease in stiffness**

**Hysteretic loop**

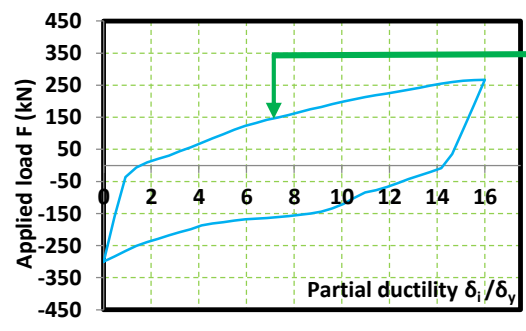
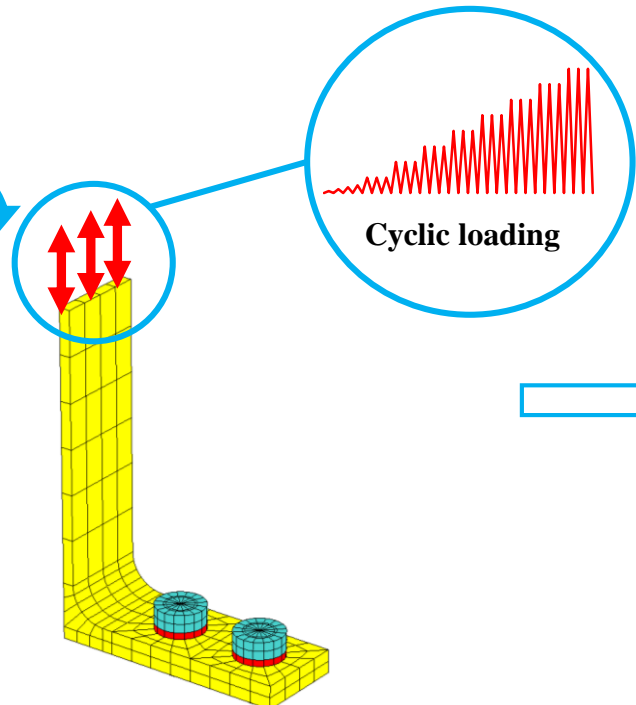


**Uplift of the end part**

**Deformed shape**

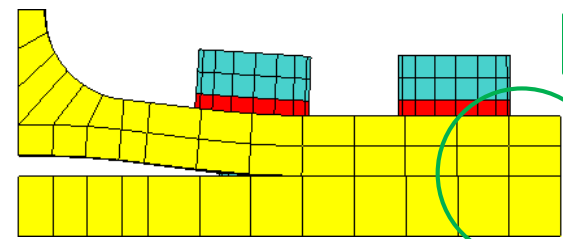


**T-stub with 4 bolts**



**No significant decrease in stiffness**

**Hysteretic loop**



**No uplift of the end part**

**Deformed shape**